

# Heavy neutral leptons from kaons in effective field theory

Rebeca Beltrán,<sup>a</sup> Julian Günther,<sup>b</sup> Martin Hirsch,<sup>a</sup> Arsenii Titov,<sup>c</sup>  
Zeren Simon Wang<sup>d,e</sup>

<sup>a</sup>*AHEP Group, Instituto de Física Corpuscular – CSIC/Universitat de València, Apartado 22085, E-46071 València, Spain*

<sup>b</sup>*Bethe Center for Theoretical Physics & Physikalisches Institut der Universität Bonn, Nußallee 12, 53115 Bonn, Germany*

<sup>c</sup>*Dipartimento di Fisica “Enrico Fermi”, Università di Pisa and INFN, Sezione di Pisa, Largo Bruno Pontecorvo 3, I-56127 Pisa, Italy*

<sup>d</sup>*Department of Physics, National Tsing Hua University, Hsinchu 300, Taiwan*

<sup>e</sup>*Center for Theory and Computation, National Tsing Hua University, Hsinchu 300, Taiwan*  
*E-mail: [rebeca.beltran@ific.uv.es](mailto:rebeca.beltran@ific.uv.es), [guenther@physik.uni-bonn.de](mailto:guenther@physik.uni-bonn.de), [mahirsch@ific.uv.es](mailto:mahirsch@ific.uv.es), [arsenii.titov@df.unipi.it](mailto:arsenii.titov@df.unipi.it), [wzs@mx.nthu.edu.tw](mailto:wzs@mx.nthu.edu.tw)*

**ABSTRACT:** In the framework of the low-energy effective theory containing in addition to the Standard Model fields heavy neutral leptons (HNLs), we compute the decay rates of neutral and charged kaons into HNLs. We consider both lepton-number-conserving and lepton-number-violating four-fermion operators, taking into account also the contribution of active-heavy neutrino mixing. Assuming that the produced HNLs are long-lived, we perform simulations and calculate the sensitivities of future long-lived-particle (LLP) detectors at the high-luminosity LHC as well as the near detector of the Deep Underground Neutrino Experiment (DUNE-ND) to the considered scenario. When applicable, we also recast the existing bounds on the minimal mixing case obtained by NA62, T2K, and PS191. Our findings show that while the future LHC LLP detectors can probe currently allowed parameter space only in certain benchmark scenarios, DUNE-ND should be sensitive to parameter space beyond the current bounds in almost all the benchmark scenarios and for some of the effective operators considered it can even probe new-physics scales in excess of 3000 TeV.

---

## Contents

<b>1</b>	<b>Introduction</b>	<b>1</b>
<b>2</b>	<b>HNLs from kaons in effective field theory</b>	<b>3</b>
2.1	The neutral kaon system	3
2.2	Effective field theory with right-handed neutrinos	4
2.3	HNL production in kaon decays	5
<b>3</b>	<b>Experiments and simulation</b>	<b>8</b>
<b>4</b>	<b>Results</b>	<b>12</b>
<b>5</b>	<b>Summary</b>	<b>19</b>
<b>A</b>	<b>Kaon decays into HNLs</b>	<b>20</b>
A.1	Form factors	20
A.2	Two-body decays	21
A.3	Three-body decays	22
<b>B</b>	<b>HNL decays</b>	<b>24</b>

---

## 1 Introduction

A rich program of searches for long-lived particles (LLPs) is planned at the LHC in the next decades [1–3]. It envisions the construction of several dedicated experiments sensitive to decay lengths of  $\mathcal{O}(1 - 100)$  m. Some LLP detectors, namely, FASER [4, 5] and MoEDAL-MAPP1 [6, 7], are already operational, whereas several more experiments are planned for the high-luminosity (HL) phase of the LHC. These include ANUBIS [8], CODEX-b [9], FACET [10], FASER2 [3], MoEDAL-MAPP2 [6, 7], and MATHUSLA [1, 11, 12]. Besides, the Deep Underground Neutrino Experiment (DUNE) [13–17] presently under construction will allow searching for light LLPs with its near detector (DUNE-ND) [18] at Fermilab as well.

LLPs are present in many models that can account for unresolved problems in particle physics and cosmology, such as the mechanism of neutrino mass generation and the nature of dark matter. The main focus of phenomenological studies so far has been on various renormalizable models, including the Higgs portal, the neutrino portal, the dark photon portal, as well as on non-renormalizable models featuring long-lived axion-like particles (ALPs), see *e.g.* Refs. [3, 19] for reviews and references.

However, it is plausible that in addition to the renormalizable couplings, LLPs may interact with the Standard Model (SM) via effective, non-renormalizable interactions. In this case, the SM viewed as an effective field theory (EFT) has to be extended to include LLPs and their effective interactions. One such example is the  $N_R$ SMEFT [20–23], which assumes the existence of heavy neutral leptons (HNLs),  $N$ , with masses below or around the electroweak scale,  $v$ . Recently, a dictionary of tree-level UV completions of the dimension-six and dimension-seven operators with  $N_R$  has been provided in Ref. [24].

There are two basic ways of HNL production at the LHC: (i) directly from partonic collisions, and (ii) for  $m_N \leq$  (few) GeV, in decays of mesons, which in turn are copiously produced in  $pp$  collisions. The latter way is also the dominant production channel of the HNLs at the DUNE experiment. Long-lived HNLs produced in the first way via the four-fermion operators with two quarks and either two or one  $N_R$  have been studied in Ref. [25] and Ref. [26], respectively. These two sets of effective operators lead to distinct phenomenology. The pair- $N_R$  operators may enhance the production cross section while not contributing to the decay of the lightest HNL. This makes the far LLP detectors introduced above an ideal place to probe such effective interactions [25]. On the contrary, single- $N_R$  operators, if large enough to enhance the HNL production, will also induce HNL decays. Still, displaced-vertex searches at the local LHC detectors (ATLAS and CMS) are very efficient to probe this set of effective operators [26]. The reach of the LLP detectors to the neutrino dipole operator involving an active neutrino and  $N_R$  has been recently estimated in Ref. [27]. Instead, Ref. [28] has revisited the LEP limits on the dimension-five sterile neutrino dipole operator (existing for at least two generations of HNLs,  $N_1$  and  $N_2$ ), taking into account active-heavy neutrino mixing.

Meson decays into long-lived HNLs triggered by non-renormalizable interactions have been considered in Refs. [29–33]. The EFT appropriate for the description of meson decays is  $N_R$ LEFT [34–37], the low-energy theory where the top quark, the Higgs boson and the heavy  $SU(2)_L$  gauge bosons are not present as dynamical degrees of freedom. In Ref. [29], the authors have investigated the reach of the proposed LHC far detectors to HNLs produced in the decays of  $D$ - and  $B$ -mesons via single- $N_R$  operators with a charged lepton, demonstrating that the new physics scale,  $\Lambda$ , as high as 100 TeV could be probed by these detectors. The same set of single- $N_R$  operators, but with the  $\tau$  lepton, would lead to HNL production in  $\tau$  decays at Belle II [38] (see also Ref. [39]). Pair- $N_R$  operators triggering  $D$ - and  $B$ -meson decays have been thoroughly examined in Ref. [30]. It has been shown that for certain operators  $\Lambda$  as large as 300 TeV and active-heavy neutrino mixing squared,  $|U_{eN}|^2$ , as small as  $10^{-15}$  could be tested by MATHUSLA, with the reach of ANUBIS being only a factor of a few smaller. In Ref. [31], the sensitivities of FASER2, FACET, ANUBIS, CODEX-b, and MAPP, to the dimension-five sterile neutrino dipole operator have been estimated. This operator leads to two-body decays of vector mesons into  $N_1$  and  $N_2$  mediated by a photon,  $\gamma$ , and a subsequent decay of the heavier HNL  $N_2 \rightarrow N_1\gamma$ . Similarly, the sensitivity reach of FASER2 and FACET to the dipole operator coupling an HNL to the photon has recently been investigated in Ref. [32] for the HNLs produced

from meson decays. Furthermore, Ref. [33] studied the sensitivity reach of the DUNE-ND (as well as the LHC far detectors) to the HNLs produced from decays of mesons including kaons, both in the minimal scenario and in the EFT, emphasizing on the feasibility of using the  $N_R$ SMEFT to describe not only the HNLs but also the lightest neutralinos in the R-parity-violating supersymmetry.

In the present work, we perform state-of-the-art numerical simulations and derive the sensitivities of the future LLP detectors at the LHC as well as the DUNE-ND<sup>1</sup> to HNLs produced from neutral and charged kaon decays in the  $N_R$ LEFT.<sup>2</sup> First, we study the scenario in which the HNL production is induced by pair- $N_R$  operators, while the HNL decay proceeds via active-heavy neutrino mixing  $U_{eN}$ . Second, we investigate the case in which both HNL production and decay are induced by the same single- $N_R$  operator structure, but with different quark flavor indices. Finally, we consider the situation where the production proceeds via a single- $N_R$  operator as well as via  $U_{eN}$ , while the  $N$  decays via mixing only. We consider both lepton-number-conserving (LNC) and lepton-number-violating (LNV) operators and discuss the differences.

HNLs can also mediate meson decays. In particular, LNV decays  $K^\mp \rightarrow \pi^\pm \ell^\mp \ell^\mp$  mediated by light sterile neutrinos have been studied in Ref. [45] adopting the EFT approach. We also mention Ref. [46]. Here, the authors have derived limits on EFT operators from HNL searches in kaon decays (among others).

The remainder of the paper is organized as follows. In Sec. 2, we briefly recap neutral kaon mixing, summarize the  $N_R$ LEFT operators of interest, and then discuss the HNL production from kaon decays. In Sec. 3, we describe various experiments we consider and provide the details of numerical simulations. Sec. 4 contains the derived sensitivities and the relevant discussion. Finally, we provide summary and conclusions of our work in Sec. 5. Additionally, we add two appendices at the end of the paper which explain in detail the computation of the decay widths of the kaons into the HNLs and those of the HNLs into a charged lepton and a pion, in the EFT framework.

## 2 HNLs from kaons in effective field theory

### 2.1 The neutral kaon system

The neutral kaons  $K^0$  ( $d\bar{s}$ ) and  $\bar{K}^0$  ( $s\bar{d}$ ) are flavor eigenstates that can be produced in strong interactions. Weak interactions cause the mixing between these two neutral states. If  $CP$  were a symmetry of the total hamiltonian  $\mathcal{H}$  (including strong, electromagnetic, and weak interactions),  $CP$  eigenstates would also be eigenstates of  $\mathcal{H}$ . With the convention (see *e.g.* Ref. [47])

$$\widehat{CP}|K^0\rangle = -|\bar{K}^0\rangle, \quad \widehat{CP}|\bar{K}^0\rangle = -|K^0\rangle, \quad (2.1)$$

<sup>1</sup>We note that the recently approved experiment SHiP [40–42] is expected to have less constraining power than DUNE for LLPs produced in kaon decays, and is hence not considered in this work.

<sup>2</sup>Leptonic and semi-leptonic decays of kaons in the minimal “3+1” case have been studied in detail in Ref. [43]. For a systematic study of  $K \rightarrow \pi\nu\bar{\nu}$  in the LEFT (without right-handed neutrinos), see Ref. [44].

LNC operators			LNV operators		
Name	Structure	$N_{\text{pars}}$	Name	Structure	$N_{\text{pars}}$
$\mathcal{O}_{dN}^{V,RR}$	$(\bar{d}_R \gamma_\mu d_R) (\bar{N}_R \gamma^\mu N_R)$	9	$\mathcal{O}_{dN}^{S,RR}$	$(\bar{d}_L d_R) (\bar{N}_R^c N_R)$	18
$\mathcal{O}_{uN}^{V,RR}$	$(\bar{u}_R \gamma_\mu u_R) (\bar{N}_R \gamma^\mu N_R)$	4	$\mathcal{O}_{uN}^{S,RR}$	$(\bar{u}_L u_R) (\bar{N}_R^c N_R)$	8
$\mathcal{O}_{dN}^{V,LR}$	$(\bar{d}_L \gamma_\mu d_L) (\bar{N}_R \gamma^\mu N_R)$	9	$\mathcal{O}_{dN}^{S,LR}$	$(\bar{d}_R d_L) (\bar{N}_R^c N_R)$	18
$\mathcal{O}_{uN}^{V,LR}$	$(\bar{u}_L \gamma_\mu u_L) (\bar{N}_R \gamma^\mu N_R)$	4	$\mathcal{O}_{uN}^{S,LR}$	$(\bar{u}_R u_L) (\bar{N}_R^c N_R)$	8

**Table 1.** Four-fermion operators in  $N_R$ LEFT, involving two quarks and two  $N_R$ 's, assuming one generation of  $N_R$ . LNV operator structures require “+h.c.”. In the third column, we provide the number of independent real parameters,  $N_{\text{pars}}$ , associated with each operator structure.

we can define the  $CP$  eigenstates as:

$$|K_1\rangle = \frac{1}{\sqrt{2}} (|K^0\rangle - |\bar{K}^0\rangle), \quad |K_2\rangle = \frac{1}{\sqrt{2}} (|K^0\rangle + |\bar{K}^0\rangle), \quad (2.2)$$

where the former has  $CP = +1$  and the latter  $CP = -1$ . However,  $CP$  is mildly violated by weak interactions and therefore the mass eigenstates  $|K_S\rangle$  and  $|K_L\rangle$ , characterized by definite lifetimes, are different from  $|K_1\rangle$  and  $|K_2\rangle$ :

$$|K_S\rangle = \frac{|K_1\rangle + \varepsilon|K_2\rangle}{\sqrt{1 + |\varepsilon|^2}}, \quad |K_L\rangle = \frac{|K_2\rangle + \varepsilon|K_1\rangle}{\sqrt{1 + |\varepsilon|^2}}, \quad (2.3)$$

where  $\varepsilon$  is the parameter accounting for indirect  $CP$  violation in neutral kaon decays.  $K_S$  ( $K_L$ ) denotes the neutral kaon with the shorter (longer) lifetime. Experimentally,  $|\varepsilon| \approx 2.23 \times 10^{-3}$  [48], and for the purposes of this work we can safely neglect it. Thus, in what follows we assume  $|K_S\rangle \approx |K_1\rangle$  and  $|K_L\rangle \approx |K_2\rangle$ .

## 2.2 Effective field theory with right-handed neutrinos

We will work in the framework of the low-energy effective field theory extended with right-handed neutrinos,  $N_R$ , dubbed as  $N_R$ LEFT, see *e.g.* [34–37]. We assume  $N_R$  to be a Majorana particle and allow for both lepton-number-conserving (LNC) and lepton-number-violating (LNV) operators. Charm and bottom meson decays triggered by four-fermion effective operators with  $N_R$  have been studied in detail in Refs. [29, 30]. Here, we are interested in the decays of kaons induced by four-fermion interactions. These interactions can be grouped into pair- $N_R$  operators given in table 1 and single- $N_R$  operators provided in table 2.<sup>3</sup> Since the top quark is not in the spectrum of the  $N_R$ LEFT, we have  $n_u = 2$  and  $n_d = n_e = n_\nu = 3$ , with  $n_f$  denoting the number of generations of a fermion  $f$ . In addition, we assume one generation of  $N_R$ .

<sup>3</sup>In what follows, we will not consider single- $N_R$  operators with an active neutrino  $\nu_L$ .

LNC operators		LNV operators	
Name	Structure	Name	Structure
$\mathcal{O}_{udeN}^{V,RR}$	$(\overline{u}_R \gamma_\mu d_R) (\overline{e}_R \gamma^\mu N_R)$	$\mathcal{O}_{udeN}^{V,LL}$	$(\overline{u}_L \gamma_\mu d_L) (\overline{e}_L \gamma^\mu N_R^c)$
$\mathcal{O}_{udeN}^{V,LR}$	$(\overline{u}_L \gamma_\mu d_L) (\overline{e}_R \gamma^\mu N_R)$	$\mathcal{O}_{udeN}^{V,RL}$	$(\overline{u}_R \gamma_\mu d_R) (\overline{e}_L \gamma^\mu N_R^c)$
$\mathcal{O}_{udeN}^{S,RR}$	$(\overline{u}_L d_R) (\overline{e}_L N_R)$	$\mathcal{O}_{udeN}^{S,LL}$	$(\overline{u}_R d_L) (\overline{e}_R N_R^c)$
$\mathcal{O}_{udeN}^{T,RR}$	$(\overline{u}_L \sigma_{\mu\nu} d_R) (\overline{e}_L \sigma^{\mu\nu} N_R)$	$\mathcal{O}_{udeN}^{T,LL}$	$(\overline{u}_R \sigma_{\mu\nu} d_L) (\overline{e}_R \sigma^{\mu\nu} N_R^c)$
$\mathcal{O}_{udeN}^{S,LR}$	$(\overline{u}_R d_L) (\overline{e}_L N_R)$	$\mathcal{O}_{udeN}^{S,RL}$	$(\overline{u}_L d_R) (\overline{e}_R N_R^c)$

**Table 2.** Four-fermion operators in  $N_R$ LEFT, involving two quarks, one charged lepton, and one  $N_R$ . Both LNC and LNV operator structures require “+h.c.”. For one generation of  $N_R$ , there are 36 independent real parameters associated with each operator structure.

Generically,  $N_R$  mixes with the active neutrinos at the renormalizable level. Integrating out the  $W$  boson leads to the following contribution to the effective Lagrangian:

$$\mathcal{L}_{\text{mix}} = -\frac{4G_F}{\sqrt{2}} V_{ij} U_{\ell N} (\overline{u}_{iL} \gamma_\mu d_{jL}) (\overline{e}_{\ell L} \gamma^\mu N_R^c) + \text{h.c.}, \quad (2.4)$$

where  $G_F$  is the Fermi constant,  $V$  is the CKM quark mixing matrix, and  $U_{\ell N}$  is active-heavy neutrino mixing. For simplicity, we will assume that the HNL mixes with the electron neutrino only, and consider the single- $N_R$  operators with the first-generation leptons only.<sup>4</sup> For charged kaon decays, the relevant CKM matrix element is  $V_{us}$ . In what follows, we will separate this contribution from the corresponding operator in table 2 by denoting its Wilson coefficient (WC) as

$$c_{\text{mix}} = -\frac{4G_F}{\sqrt{2}} V_{us} U_{\ell N}, \quad \text{with} \quad |c_{\text{mix}}| \approx \frac{0.45 |U_{\ell N}|}{v^2}. \quad (2.5)$$

For a more detailed discussion of  $N_R$ LEFT, including the running of the considered operators and their matching to the  $N_R$ SMEFT operators, see Ref. [30].

### 2.3 HNL production in kaon decays

The pair- $N_R$  operators  $\mathcal{O}_{dN}$  from table 1 involving  $d$  and  $s$  quarks trigger the following two- and three-body decays:  $K_{S/L} \rightarrow NN$ ,  $K_{S/L} \rightarrow \pi^0 NN$  and  $K^\pm \rightarrow \pi^\pm NN$ . The single- $N_R$  operators  $\mathcal{O}_{udeN}$  from table 2 containing  $u$  and  $s$  quarks induce  $K^\pm \rightarrow e^\pm N$ ,  $K^\pm \rightarrow \pi^0 e^\pm N$  and  $K_{S/L} \rightarrow \pi^\pm e^\mp N$ . In appendix A, we provide the formulae for the two-body decay widths and the three-body decay amplitudes. The three-body decay widths are then computed according to the procedure explained in Refs. [29, 30].

If the products of HNL decays are not detected, the kaon decay modes we are interested in contribute to  $K_{S/L} \rightarrow \text{inv.}$ ,  $K_{S/L} \rightarrow \pi^0 \nu \bar{\nu}$ ,  $K^\pm \rightarrow \pi^\pm \nu \bar{\nu}$ , and  $K^+ \rightarrow e^+ \nu_e$ ,  $K^+ \rightarrow$

<sup>4</sup>Since the mass of the muon is only smaller than the kaon mass by a factor  $\sim 4.7$ , the branching ratios of the kaon decays triggered by the single- $N_R$  operators with the muon will be phase-space-suppressed with respect to those into an electron and an HNL.

Decay	Branching ratio	Decay	Branching ratio
$K_L \rightarrow \pi^0 \nu \bar{\nu}$	$< 3.0 \times 10^{-9}$ at 90% C.L.	$K^+ \rightarrow e^+ \nu_e$	$(1.582 \pm 0.007) \times 10^{-5}$
$K^+ \rightarrow \pi^+ \nu \bar{\nu}$	$(1.14_{-0.33}^{+0.40}) \times 10^{-10}$	$K^+ \rightarrow \pi^0 e^+ \nu_e$	$(5.07 \pm 0.04) \times 10^{-2}$
		$K_S \rightarrow \pi^\pm e^\mp \nu_e$	$(7.04 \pm 0.08) \times 10^{-4}$
		$K_L \rightarrow \pi^\pm e^\mp \nu_e$	$(40.55 \pm 0.11) \times 10^{-2}$

**Table 3.** Branching ratios of semi-invisible kaon decays [48]. For  $K_{S/L} \rightarrow \pi^\pm e^\mp \nu_e$ , the values are for the sum of particle and antiparticle states indicated.

$\pi^0 e^+ \nu_e$ ,  $K_{S/L} \rightarrow \pi^\pm e^\mp \nu_e$ . The branching ratios of the decays into final states with at least one charged particle have been measured, whereas for  $K_L \rightarrow \pi^0 \nu \bar{\nu}$  a stringent upper limit on the branching ratio has been obtained. We summarize the current experimental results in table 3. We will take them into account when deriving the limits on the WCs of the pair- $N_R$  and single- $N_R$  operators. In the case of a measured branching ratio, we will require the new contribution not to exceed twice the experimental error, whereas for  $K_L \rightarrow \pi^0 NN$ , we will demand that its branching ratio is smaller than  $3.0 \times 10^{-9}$  in accordance with the current upper bound on the branching ratio of  $K_L \rightarrow \pi^0 \nu \bar{\nu}$  [48].

In figure 1, we display the branching ratios of kaon decays triggered by the LNC operator  $\mathcal{O}_{dN,21}^{V,RR}$  and by the LNV operator  $\mathcal{O}_{dN,21}^{S,RR}$ . In each case, we assume that the corresponding WC is either real (left panel) or purely imaginary (right panel). For the LNC operator, a real (purely imaginary) WC does not allow for  $K_S \rightarrow NN$  and  $K_L \rightarrow \pi^0 NN$  ( $K_L \rightarrow NN$  and  $K_S \rightarrow \pi^0 NN$ ), as can be inferred from eqs. (A.15) and (A.22) (eqs. (A.16) and (A.21)).<sup>5</sup> For small  $m_N$ , the allowed two-body decay is suppressed, since the corresponding decay width scales with  $m_N^2$ , see eqs. (A.15) and (A.16). In this figure, we fix the absolute value of the operator coefficient to  $10^{-6} v^{-2}$  in order to comply with the measurements reported in the left panel of table 3, in particular, with that of  $K^+ \rightarrow \pi^+ \nu \bar{\nu}$ . Switching on  $\mathcal{O}_{dN,21}^{V,LR}$  and  $\mathcal{O}_{dN,21}^{S,LR}$  (one at a time) would lead to the same results as for  $\mathcal{O}_{dN,21}^{V,RR}$  and  $\mathcal{O}_{dN,21}^{S,RR}$ , respectively.

In figure 2, we plot the branching ratios of kaon decays induced by the LNC operators  $\mathcal{O}_{udeN,12}^{V,RR}$ ,  $\mathcal{O}_{udeN,12}^{S,RR}$ , and  $\mathcal{O}_{udeN,12}^{T,RR}$ , with respective WC  $c_{\mathcal{O}}$ , as well as by active-heavy neutrino mixing  $U_{eN}$ . We show three representative cases: (i)  $U_{eN} = 10^{-5}$  and  $c_{\mathcal{O}} = 0$ , (ii)  $U_{eN} = 0$  and  $c_{\mathcal{O}} = 10^{-5} v^{-2}$ , and (iii)  $U_{eN} = 10^{-5}$  and  $c_{\mathcal{O}} = 10^{-5} v^{-2}$ . The value of the operator coefficient ensures that the branching ratios are compatible with the errors in the measurements presented in the right panel of table 3, most importantly, with that of  $K^+ \rightarrow e^+ \nu_e$ . The value  $U_{eN} = 10^{-5}$  ( $|U_{eN}|^2 = 10^{-10}$ ) is such that it is below the existing constraints. For HNLs lighter than the kaons, the leading constraints on the mixing parameter come from NA62 [49], PS191 [50], and T2K [51], which set upper limits at the level of  $|U_{eN}|^2 \sim 5 \times 10^{-10}$ . For even lighter HNLs, below the pion mass, PIENU [52] has

<sup>5</sup>We note that this is strictly true only in the limit  $\varepsilon \rightarrow 0$ .

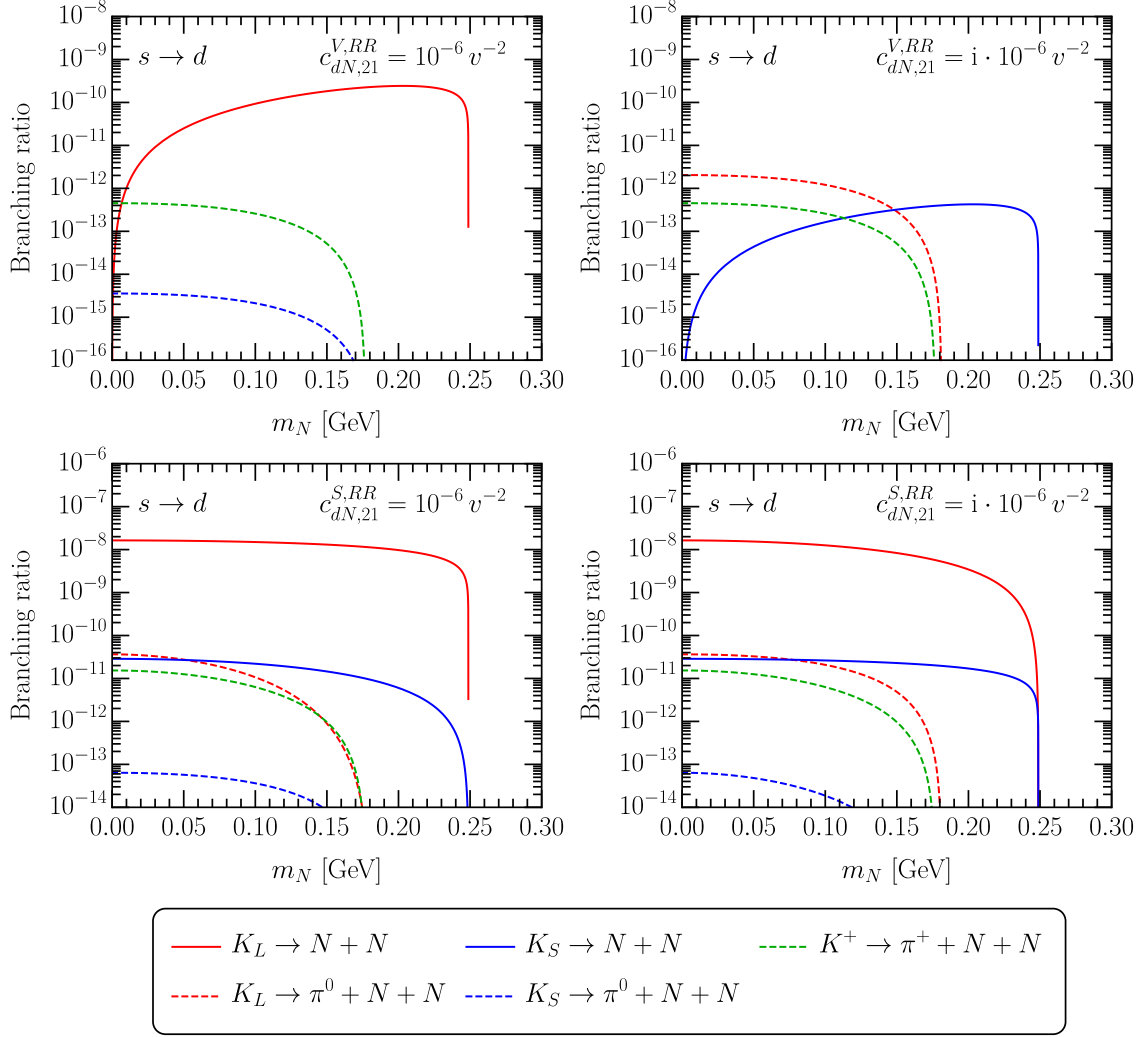


**Figure 1.** Branching ratios of kaon decays triggered by the LNC (top) and LNV (bottom) pair- $N_R$  operators. In the left (right) panel, the corresponding WC is purely real (imaginary).

ruled out parameter space corresponding to  $|U_{eN}|^2 > 10^{-7} \sim 10^{-8}$ . Moreover, with the chosen value for the mixing, its contribution is comparable to the contributions of most operators for  $c_{\mathcal{O}} \sim 10^{-5} v^{-2}$ , cf. eq. (2.5). For the scalar operator  $\mathcal{O}_{udeN,12}^{S,RR}$ , the constraints from NA62 set limits on the operator to  $c_{\mathcal{O}} \sim 10^{-6} v^{-2}$ .

In figure 3, we show the branching ratios for the same processes as in figure 2, but for the LNV operators  $\mathcal{O}_{udeN,12}^{V,RL}$ ,  $\mathcal{O}_{udeN,12}^{S,RL}$ , and  $\mathcal{O}_{udeN,12}^{T,LL}$ . In the absence of mixing, the results are identical to those for the corresponding LNC operators (switched on one at a time). In the presence of mixing, there is an interference between the effective operator generated by new physics and the four-fermion interaction (see eq. (2.4)) arising from integrating out the  $W$  boson. Its effect is more pronounced for the vector-type operators, and it is stronger for the LNV operator, as can be understood from eq. (A.17).



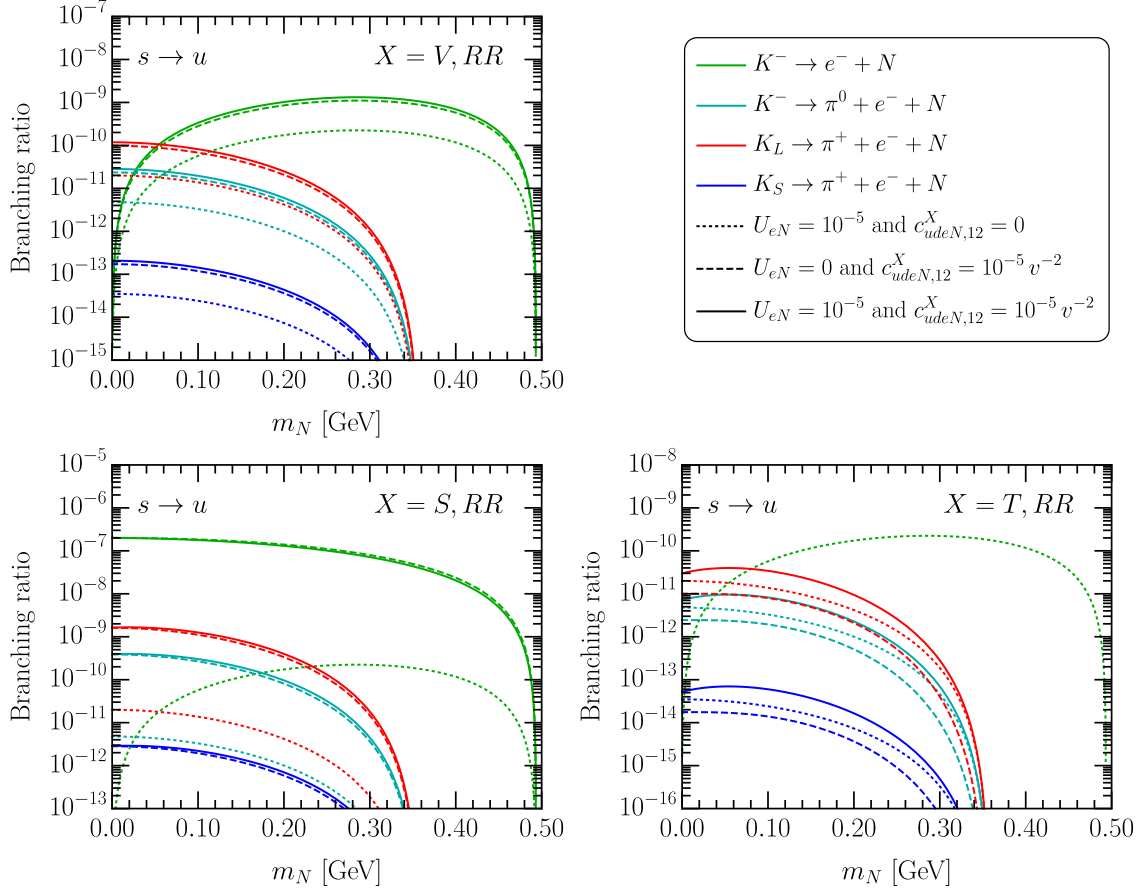


**Figure 2.** Branching ratios of kaon decays triggered by the LNC single- $N_R$  operators with electron, as well as by active-heavy mixing  $U_{eN}$ .

### 3 Experiments and simulation

A whole list of far detectors have been proposed for operation in the vicinity of various interaction points (IPs) of the LHC, either during Run 3 or the HL-LHC phase; some of them have even been approved and are running, including FASER and MoEDAL-MAPP1. Since they are all sensitive to signatures of tracks stemming from displaced decays of LLPs taking place inside their fiducial volumes, we will perform the numerical analysis taking into account these proposals comprehensively.

We classify these detectors according to their associated IP at the LHC. For the ATLAS IP, ANUBIS [8], FASER [4, 5], and FASER2 [3] are relevant. ANUBIS<sup>6</sup> is a detector proposed to be installed inside one of the service shaft above the ATLAS IP. It has a cylindrical shape of 56 m height and 18 m diameter. Being close to the ATLAS IP, it is

<sup>6</sup>Very recently, a new design of ANUBIS has been discussed [53, 54]. Instead of being placed inside one of the service shafts, ANUBIS is now considered to be installed at the ATLAS cavern ceiling or shaft bottom. Given the changing status of the proposal, we stick to the original design for sensitivity study as a good reference for interested readers.

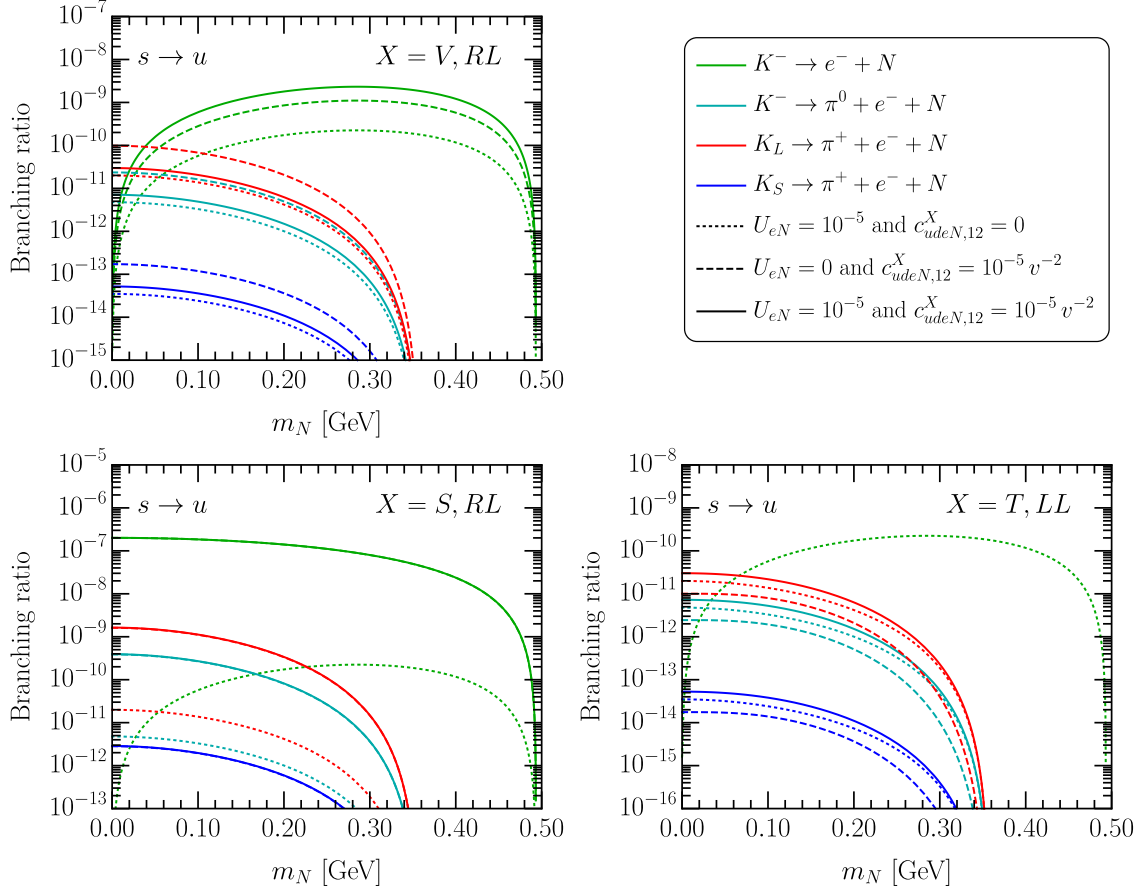


**Figure 3.** Branching ratios of kaon decays triggered by the LNV single- $N_R$  operators with electron, as well as by active-heavy mixing  $U_{eN}$ .

expected to suffer from certain background sources such as neutral kaons. Nevertheless, exclusion bounds at 95% confidence level (C.L.) are usually shown with 3 signal events, assuming zero background, and we will follow the practice in this paper. FASER is currently collecting data at the LHC; first results can be found in Refs. [55, 56]. It is a small cylindrical detector installed in the very forward position along the beam direction, with a distance of 480 m from the IP. Further, an upgraded program of FASER, FASER2, has been suggested to be built at the site of the proposed Forward Physics Facility [3]. It is larger than FASER and has hence better acceptances to LLPs. ANUBIS and FASER2 should collect in total  $3 \text{ ab}^{-1}$  integrated luminosity data, while FASER will have order of  $150 \text{ fb}^{-1}$  integrated luminosity.

Near the CMS IP, MATHUSLA [1, 11, 12] and FACET [10] have been proposed. MATHUSLA would be an experiment on the ground, with about 100 m distance from the CMS IP. It would have a huge effective volume of  $100 \text{ m} \times 100 \text{ m} \times 25 \text{ m}$ . FACET is suggested to be a sub-system of the CMS experiment; with a cylindrical shape, it has a distance of 101 m from the CMS IP, enclosing the beam pipe. Moreover, with a radius

of 0.5 m and a length of 18 m, FACET is relatively large compared to FASER. Both MATHUSLA and FACET would be running during the HL-LHC and will hence have an integrated luminosity of  $3 \text{ ab}^{-1}$ .

Finally, for the LHCb IP, we have CODEX-b [9], and MoEDAL-MAPP1 and MoEDAL-MAPP2 [6, 7]. CODEX-b has been proposed as a cubic box with a dimension of  $10 \text{ m} \times 10 \text{ m} \times 10 \text{ m}$  covering the pseudorapidity range  $[0.2, 0.6]$ , roughly 10 m away from IP8. MoEDAL-MAPP1 is a small detector of about  $140 \text{ m}^3$  in a gallery of negative pseudorapidity with respect to the LHCb IP, under operation during Run 3, and MoEDAL-MAPP2 is an enlarged version of MAPP1, to be running during the HL-LHC period. The integrated luminosity associated with the LHCb IP is lower compared to that of ATLAS or CMS. CODEX-b and MoEDAL-MAPP2 will have an integrated luminosity of  $300 \text{ fb}^{-1}$  while MoEDAL-MAPP1 has only  $30 \text{ fb}^{-1}$ .

For a more detailed summary of these proposals, we refer the reader to *e.g.* Refs. [2, 29, 57], as well as to the respective references proposing the detectors.

In addition, at DUNE, a proton beam of energy 120 GeV hits a fixed target with  $1.1 \times 10^{21}$  POTs (protons on target) expected per year. The produced mesons decay either promptly or with a macroscopic distance into the LLPs (which are the HNLs in this study) inside a decay pipe which is 26 m downstream from the IP and has a length of 194 m and a radius of 2 m. The produced LLPs should then travel a long distance before decaying inside the DUNE-ND which is further downstream with a distance of 574 m from the fixed target, and has a length of 6.4 m and a width of 3.5 m. We take an operation duration of 10 years as benchmark in this study, expecting thus in total  $1.1 \times 10^{22}$  POTs.

In order to obtain the kinematics of the HNLs produced from kaons, we make use of the tool Pythia8 with the module *SoftQCD:all*. The kaons are generated in  $pp$  collisions with a center-of-mass-energy 14 TeV, and are set to decay exclusively in the signal-event channels. Pythia8 provides the boost factor and the polar angle of each simulated HNL. We note that since kaons are themselves long-lived, we let Pythia8 decide the decay positions of the kaons and thus take into account the production position of the HNL (= the decay position of the kaon) as well as the polar angle and boost factor of the HNL, in the computation of the HNLs' average decay probability inside the far detectors. The total signal-event rates at each detector can be computed with the following formula

$$N_S = \sum_{K's} N_K \cdot n \cdot \text{BR}(K \rightarrow n N + \text{anything}) \cdot \epsilon \cdot \text{BR}(N \rightarrow \text{visible}) , \quad (3.1)$$

where the summation goes over different kaons,  $N_K$  is the total number of kaons,  $n = 1, 2$  is the number of HNLs produced in the considered kaon decays,  $\text{BR}(N \rightarrow \text{visible})$  is the visible decay branching ratio of the HNL, and  $\epsilon$  is the average decay probability in a far detector. For the LHC experiments, we estimate the number of kaons  $N_K$ , with the help of the tool EPOS LHC [58] provided in the CRMC simulation package [59], to be  $N_{K^\pm} = 2.38 \times 10^{18}$ ,  $N_{K_S} = 1.31 \times 10^{18}$ , and  $N_{K_L} = 1.30 \times 10^{18}$ , over the whole  $4\pi$  solid angle. For the DUNE experiment, we follow Refs. [33, 60] and conclude that the total

numbers of kaons produced at DUNE for 10 years are  $N_{K^\pm} = N_{K_S} = N_{K_L} = 5.76 \times 10^{21}$  over the whole  $4\pi$  solid-angle range. The computation procedure of  $\epsilon$  is based on the exact formulae given in Refs. [29, 30, 61–63] and the further development presented in Ref. [33] for LLPs from kaons. As the kaons, especially  $K^\pm$  and  $K_L$ , travel macroscopic distances, the infrastructure surrounding the IPs may affect the kinematics of the kaons. To simplify the analysis, we neglect the influence of any magnetic fields present at the LHC IPs or the magnetic horns at DUNE. Additionally, we introduce cut-offs for the production positions of the HNL at the LHC that are included in the signal-event rates  $N_S$ , resulting in conservative estimates. Here, we provide a brief summary of the cut-offs we employ in our simulation; for more detail, see Ref. [33]. For example, a lead shield covering the total fiducial volume in order to veto neutral background events is placed approximately 5 m in front of CODEX-b. Hence, we require the kaons to decay before reaching the shield. For detectors in the far forward region (FASER, FASER2, and FACET), we employ the beamline geometry of the ATLAS and CMS IP, which involve absorbers for charged and neutral particles in order to protect beamline infrastructure. The hadron calorimetry of ATLAS and CMS restricts the decay region of the kaons for ANUBIS and MATHUSLA, respectively. Lastly, for MoEDAL-MAPP1 and MAPP2, the natural rock between the IP and the detectors is the limiting factor. Hence, the kaons are required to decay within the 3.8 m wide beam cavern. We note that such cut-offs are not needed for the DUNE-ND, as a decay pipe for the long-lived mesons to decay in should be instrumented.

Finally, we discuss the procedure we apply for recasting the bounds on the HNLs in the minimal scenario, obtained in some past searches, into those on the HNLs in the EFT scenarios considered here. In general, we follow the approaches laid out in Refs. [46, 64, 65] (see also Ref. [66]). We consider three searches at NA62 [49], PS191 [50], and T2K [51]. Since these searches all require a prompt charged lepton, they are applicable only to the single- $N_R$  scenarios. We first consider the NA62 search, which looked for HNL production in  $K^+$  decays to positrons and missing energy, assuming the proper lifetime of  $N$  is larger than 50 ns. The search obtained bounds on  $\text{BR}(K^+ \rightarrow e^+ N)$  and hence those on the active-sterile neutrino mixing, as functions of the sterile neutrino mass. We simply convert  $\text{BR}(K^+ \rightarrow e^+ N)$  to the production Wilson coefficient of the single- $N_R$  scenario in question, for each mass value, and obtain the corresponding recast bounds. Both the PS191 and T2K searches are for both a prompt charged lepton and a displaced vertex at the detached detector. For PS191, we extract the sensitivity curve presented in the plane  $|U_{eN}|^2$  vs.  $m_N$  for the signal process  $K^+ \rightarrow e^+ N$ ,  $N \rightarrow e^- \pi^+$  and its charge-conjugate channel, and for the T2K near detector ND280, the signal process  $K^\pm \rightarrow e^\pm N$ ,  $N \rightarrow e^\pm \pi^\mp$  is considered. By rescaling the production and visible decay rates, we obtain the recast bounds in the EFT parameter space.

Benchmark	Production	Decay	Benchmark	Production	Decay
B1.1	$c_{dN,21}^{V,RR} \in \mathbb{R}$	$U_{eN}$	B3	$c_{udeN,12}^{V,RR}$	$c_{udeN,11}^{V,RR}$
B1.2	$c_{dN,21}^{V,RR} \in i\mathbb{R}$	$U_{eN}$	B4	$c_{udeN,12}^{S,RR}$	$c_{udeN,11}^{S,RR}$
B2.1	$c_{dN,21}^{S,RR} \in \mathbb{R}$	$U_{eN}$	B5	$c_{udeN,12}^{V,RR}$ and $U_{eN}$	$U_{eN}$
B2.2	$c_{dN,21}^{S,RR} \in i\mathbb{R}$	$U_{eN}$	B6	$c_{udeN,12}^{S,RR}$ and $U_{eN}$	$U_{eN}$
			B7	$c_{udeN,12}^{V,RL}$ and $U_{eN}$	$U_{eN}$
			B8	$c_{udeN,12}^{S,RL}$ and $U_{eN}$	$U_{eN}$

**Table 4.** Benchmarks for the scenarios with pair- $N_R$  (left) and single- $N_R$  (right) operators.

## 4 Results

For presenting the numerical results, we choose several benchmarks characterized by the different couplings responsible for the HNL production and decay. We summarize them in table 4. In total, we consider four scenarios with pair- $N_R$  operators (benchmarks B1 and B2, each having two sub-cases) and six scenarios with single- $N_R$  operators (benchmarks B3–B8).

For benchmark B1 (B2), HNL production is governed by the LNC (LNV) pair- $N_R$  operator  $\mathcal{O}_{dN,21}^{V,RR}$  ( $\mathcal{O}_{dN,21}^{S,RR}$ ), while HNL decay proceeds via active-heavy neutrino mixing  $U_{eN}$ . For each of these two operators, we consider two cases: (i) real WC and (ii) purely imaginary WC, *cf.* figure 1 and the related discussion. First, in figure 4, we fix the absolute value of the WC to  $10^{-6}v^{-2}$  (to respect the constraint coming from  $K^+ \rightarrow \pi^+\nu\bar{\nu}$ ) and display the projected exclusion limits in the plane  $|U_{eN}|^2$  vs.  $m_N$  for three signal events. The curves correspond to 95% C.L. limits (under the assumption of zero background). For the LNC operator, the sensitivities are approximately two orders of magnitude weaker in the case of purely imaginary WC (B1.2, top-right plot) than in the case of real WC of the same size (B1.1, top-left plot). This can be understood from figure 1, which shows that for the same size of the WC,  $\text{BR}(K_S \rightarrow NN)$  is about two orders of magnitude smaller than  $\text{BR}(K_L \rightarrow NN)$ , whereas the production numbers of  $K_S$  and  $K_L$  are nearly the same. The difference in the sensitivities is much milder for the LNV operator, for which the branching ratios of the relevant kaon decays differ only slightly between the cases of real and purely imaginary WC.

Among the considered LLP detectors, the best limit comes from MATHUSLA, which can probe  $|U_{eN}|^2$  down to  $4 \times 10^{-8}$  ( $1.4 \times 10^{-9}$ ) at  $m_N \approx 0.23$  GeV for B1.1 (B2.1). It is followed by ANUBIS, which has a factor of a few weaker sensitivity. MAPP2, FACET and CODEX-b provide very similar exclusion limits, which are approximately two orders of magnitude weaker than the expected limits from MATHUSLA. Finally, FASER2 and

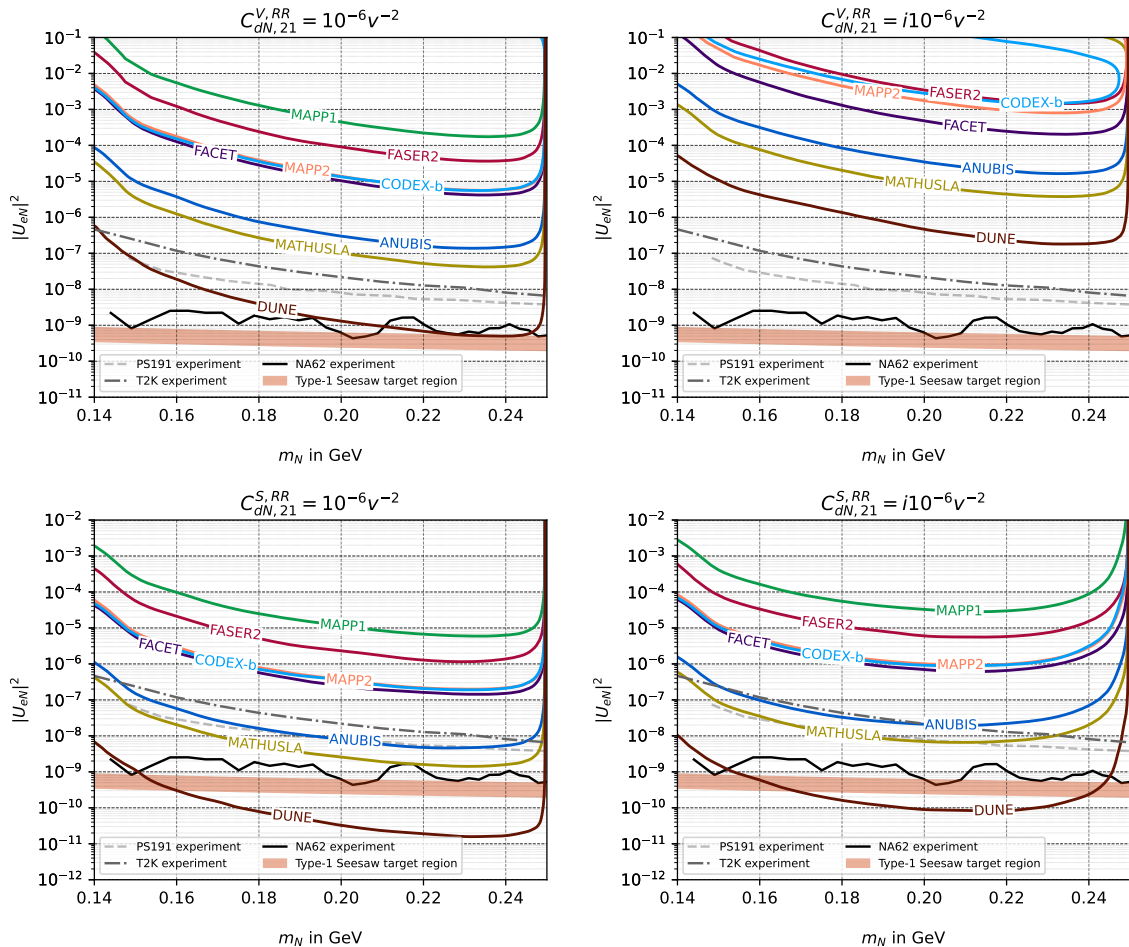


**Figure 4.** Projected exclusion limits in the plane  $|U_{eN}|^2$  vs.  $m_N$  for pair- $N_R$  operator benchmarks B1.1 and B1.2 (top), and B2.1 and B2.2 (bottom). The absolute value of the corresponding WC has been fixed to  $10^{-6}v^{-2}$ . The current bounds from NA62, T2K, and PS191, as well as the type-I seesaw target region where  $m_\nu = 0.05\text{--}0.12$  eV, are also shown.

MAPP1 have the weakest depicted sensitivities.<sup>7</sup> However, all the LHC far detectors are incomparable to the DUNE-ND which can probe  $|U_{eN}|^2$  down to the levels stronger than MATHUSLA by up to two orders of magnitude in these scenarios. This superior performance is mainly due to the much larger production rates of the kaons at DUNE. We also show the existing limits on active-heavy neutrino mixing obtained by the NA62 [49], T2K [51], and PS191 [50] experiments. Though derived under the hypothesis of the minimal mixing case, these limits apply to the considered EFT scenarios as well. As can be seen, NA62 outperforms all the LHC far detectors and already touches the (naive) type-I seesaw band, where the values of  $m_N$  and  $U_{eN}$  yield the light neutrino mass  $m_\nu = 0.05\text{--}0.12$  eV.

<sup>7</sup>For FASER, there is no isocurve shown in figure 4 and figure 5. Because of the small geometric acceptance and comparatively lower integrated luminosity, the simulated number of signal events is less than three in the shown parameter region.

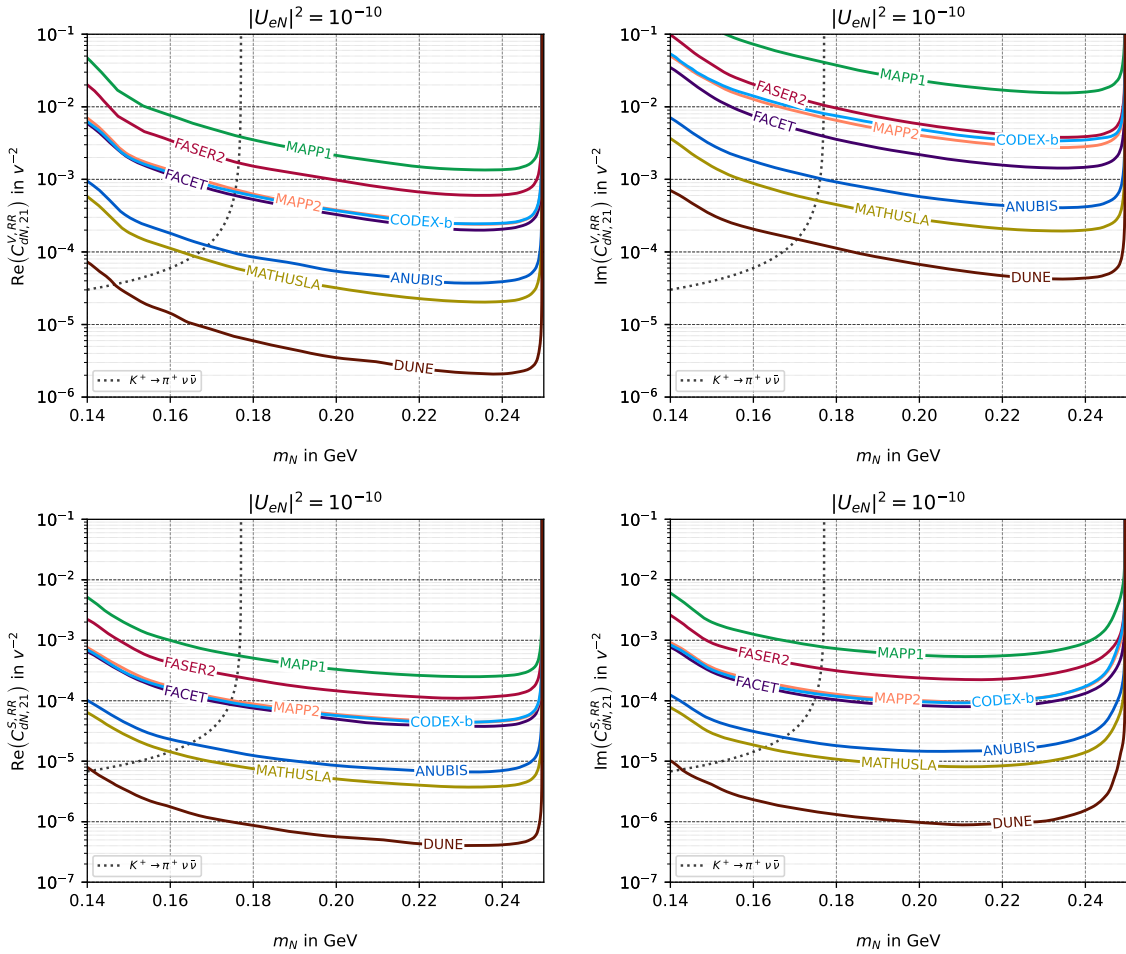


**Figure 5.** Exclusion limits in the plane WC vs.  $m_N$  for pair- $N_R$  operator benchmarks B1.1 and B1.2 (top), and B2.1 and B2.2 (bottom). The active-heavy neutrino mixing parameter has been fixed as  $|U_{eN}|^2 = 10^{-10}$ . The dotted line represents the constraint originating from the measured branching ratio of  $K^+ \rightarrow \pi^+ \nu \bar{\nu}$ .

We find that the DUNE-ND can still be sensitive to parameter space beyond the current bounds, especially in the scenarios of the benchmark B2, where it covers the type-I seesaw band.

In figure 5, we fix  $|U_{eN}|^2 = 10^{-10}$  and show the exclusion limits in the plane WC vs.  $m_N$ . For benchmark B1.1 (B1.2), MATHUSLA will be able to probe the WC as small as  $2 \times 10^{-5} v^{-2}$  ( $2 \times 10^{-4} v^{-2}$ ) for  $m_N$  in the range 0.22–0.24 GeV. These numbers translate to the new physics scale  $\Lambda$  of 55 (17) TeV.<sup>8</sup> For DUNE-ND, the sensitivity reach

<sup>8</sup>We associate the new physics scale  $\Lambda$  with the effective operators in the  $N_R$ SMEFT, assuming their WCs are  $\Lambda^{4-d}$ , with  $d$  denoting the operator mass dimension. The LNC four-fermion operators in the  $N_R$ LEFT arise from  $d = 6$  four-fermion operators in the  $N_R$ SMEFT, whereas the LNV four-fermion operators in the  $N_R$ LEFT originate from  $d = 7$  operators in the  $N_R$ SMEFT. For details of the matching between the two effective theories, see *e.g.* Refs. [29, 30, 67].

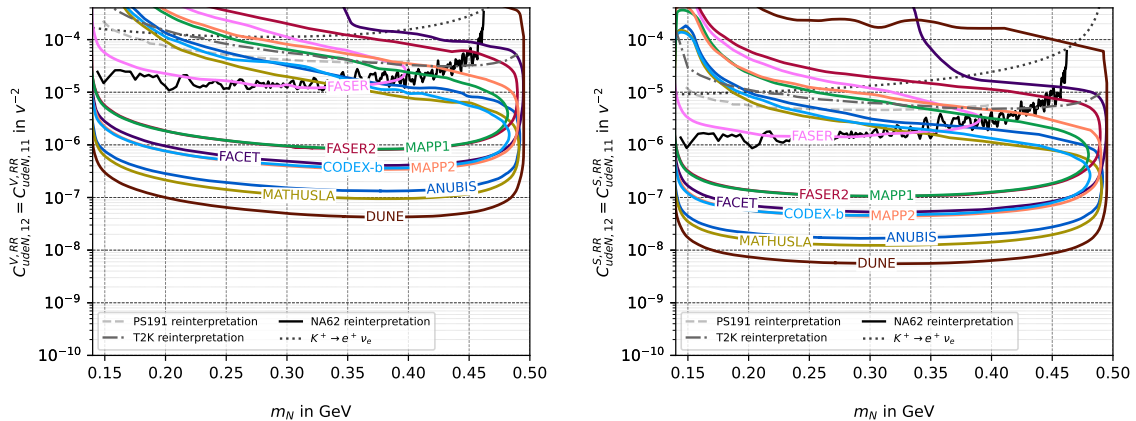


**Figure 6.** Exclusion limits in the plane WC vs.  $m_N$  for single- $N_R$  operator benchmarks B3 (left) and B4 (right). The production and decay couplings have been assumed to be equal. The recast bounds from NA62, T2K, and PS191, as well as the constraint originating from the measured branching ratio of  $K^+ \rightarrow e^+ \nu_e$ , are also shown.

can be further down to  $2 \times 10^{-6} v^{-2}$  ( $4 \times 10^{-5} v^{-2}$ ), corresponding to 174 (39) TeV. In the case of the LNV operator, we find that for benchmark B2.1 (B2.2), MATHUSLA can exclude the effective couplings down to  $4 \times 10^{-6} v^{-2}$  for  $m_N \approx 0.23$  GeV ( $8 \times 10^{-6} v^{-2}$  for  $m_N \approx 0.21$  GeV). However, being an LNV operator, it originates at dimension 7 in the  $N_R$ SMEFT, and hence, these exclusion limits translate to  $\Lambda$  of around 11 (9) TeV. DUNE-ND performs better than the LHC far detectors again, reaching  $4 \times 10^{-7} v^{-2}$  ( $8 \times 10^{-7} v^{-2}$ ) in the benchmark B2.1 (B2.2), corresponding to the new-physics scales of around 24 TeV (19 TeV) at  $m_N = 0.23$  GeV (0.21 GeV). We also show the constraint originating from the measurement of the branching ratio of  $K^+ \rightarrow \pi^+ \nu \bar{\nu}$ . It is complementary to the projected limits for  $m_N \lesssim 0.16$ – $0.17$  GeV. We recall that the NA62, PS191, and T2K exclusion limits on active-heavy mixing cannot be reinterpreted into the limits on the WCs of the pair- $N_R$  operators, since these interactions do not lead to a prompt charged lepton.

Next, we consider the single- $N_R$  operator benchmarks summarized in the right part of table 4. We start with benchmarks B3 and B4, for which we assume that both HNL production and decay proceed via the same effective operator, but carrying different quark flavor indices. The indices 12 lead to the HNL production in kaon decays, while the indices 11 realize the decay  $N \rightarrow e^\mp \pi^\pm$ . For these benchmarks, we also assume that there is no active-heavy neutrino mixing. We consider two single- $N_R$  operators  $\mathcal{O}_{udeN}^{V,RR}$  and  $\mathcal{O}_{udeN}^{S,RR}$ , both conserving the lepton number. (The results for the corresponding LNV operators are the same under the assumption of zero active-heavy neutrino mixing.) For graphical presentation, we choose to set the production and decay couplings equal, *i.e.*  $c_{udeN,12}^{V,RR} = c_{udeN,11}^{V,RR}$  for B3, and  $c_{udeN,12}^{S,RR} = c_{udeN,11}^{S,RR}$  for B4, and show the derived exclusion limits in the plane WC vs.  $m_N$ , see figure 6. In addition to the sensitivities of the proposed LLP detectors at the LHC and the DUNE-ND, we show the recast bounds from NA62 [49], T2K [51], and PS191 [50], obtained according to the procedure explained at the end of



Sec. 3. Except for FASER, of which the sensitivity is comparable to that of NA62, all the far detectors at the LHC and the DUNE-ND will have better reach to these scenarios than NA62, which excludes WC values larger than approximately  $(1-2)\times 10^{-5}v^{-2}$  ( $(9-20)\times 10^{-7}v^{-2}$ ) for benchmark B3 (B4). For the vector-type operator and  $m_N \approx 0.35-0.40$  GeV, DUNE-ND and MATHUSLA will probe the effective couplings as small as  $4 \times 10^{-8}v^{-2}$  and  $9.5 \times 10^{-8}v^{-2}$ , respectively, and FASER down to  $1.4 \times 10^{-5}v^{-2}$ , with the sensitivities of the other experiments lying between these extremes. Translating these numbers to the new-physics scale  $\Lambda$ , we find that DUNE (MATHUSLA, FASER) will be sensitive to  $\Lambda$  as high as 1230 (798, 65) TeV. For the scalar-type operator, the reach in the  $N_R$ LEFT WC is around one order of magnitude better, owing to the larger branching ratio of  $K^\pm \rightarrow e^\pm N$  in this case, see figure 2. The new-physics scales, which could be probed by DUNE (MATHUSLA, FASER) for  $m_N \approx 0.25-0.35$  GeV, are in excess of 3000 (2000, 200) TeV. The projected limits from DUNE and MATHUSLA are approximately more than ten times more stringent than the limits derived on the effective interactions in Ref. [45] from the LNV decays  $K^\mp \rightarrow \pi^\pm \ell^\mp \ell^\mp$  mediated by  $N$ .

Finally, we turn to benchmarks B5–B8, where both an effective operator and active-heavy neutrino mixing contribute to HNL production, while the HNL decay proceeds via mixing only, see table 4. Here, we consider both LNC vector (B5) and scalar (B6) operators, and LNV vector (B7) and scalar (B8) operators, since the interference between the effective interaction and the mixing term is slightly different in the LNC and LNV cases, *cf.* figures 2 and 3. In figure 7, we fix the corresponding WC to either  $10^{-5}v^{-2}$  for vector operators (to satisfy the constraint coming from  $K^+ \rightarrow e^+ \nu_e$ ), or  $10^{-6}v^{-2}$  for scalar operators (to satisfy the recast bounds from NA62), and present the sensitivities in the plane  $|U_{eN}|^2$  vs.  $m_N$ . For the vector-type operators and  $m_N \approx 0.35-0.40$  GeV, MATHUSLA could probe  $|U_{eN}|^2$  down to  $3.0$  ( $2.0$ )  $\times 10^{-10}$  for the LNC (LNV) operator, while DUNE can be sensitive to the  $|U_{eN}|^2$  values as low as  $2 \times 10^{-11}$  ( $1.5 \times 10^{-11}$ ). For the scalar-type operators in the same  $m_N$ -range, the MATHUSLA reach is  $|U_{eN}|^2 \approx 9.0$  ( $4.0$ )  $\times 10^{-10}$  for the LNC (LNV) operator and the DUNE reach to  $|U_{eN}|^2$  is down to approximately  $4 \times 10^{-10}$  ( $3 \times 10^{-11}$ ).

We also display the recast bounds from NA62, T2K, and PS191. The NA62 limit is more stringent than the expected limits from the future LLP detectors for  $m_N \lesssim 0.35$  (0.41) GeV in B5 and B8 (B6 and B7). For larger  $m_N$ , MATHUSLA takes over, excluding new parts of the parameter space. In particular, for B7, the projected MATHUSLA exclusion limits can probe the seesaw target region for  $0.25$  GeV  $\lesssim m_N \lesssim 0.45$  GeV. DUNE can, however, probe  $|U_{eN}|^2$  values smaller than the current bounds by up to about 2 orders of magnitude, in B5, B7, and B8 benchmarks. For B6, (only) DUNE can exclude a small part of the parameter space at  $m_N \gtrsim 0.4$  GeV.

In figure 8, we fix  $|U_{eN}|^2 = 10^{-10}$  and show the exclusion limits in the plane WC vs.  $m_N$ . We again depict recast bounds from NA62, T2K, and PS191. The recast NA62 bound covers the ranges which will be accessible to the future LLP detectors for  $m_N \lesssim 0.45$  GeV. For larger HNL masses, MATHUSLA will probe an unexplored region of the parameter space, ruling out the WC  $\gtrsim 2 \times 10^{-5}v^{-2}$  ( $\gtrsim 3 \times 10^{-6}v^{-2}$ ) for the vector-type (scalar-

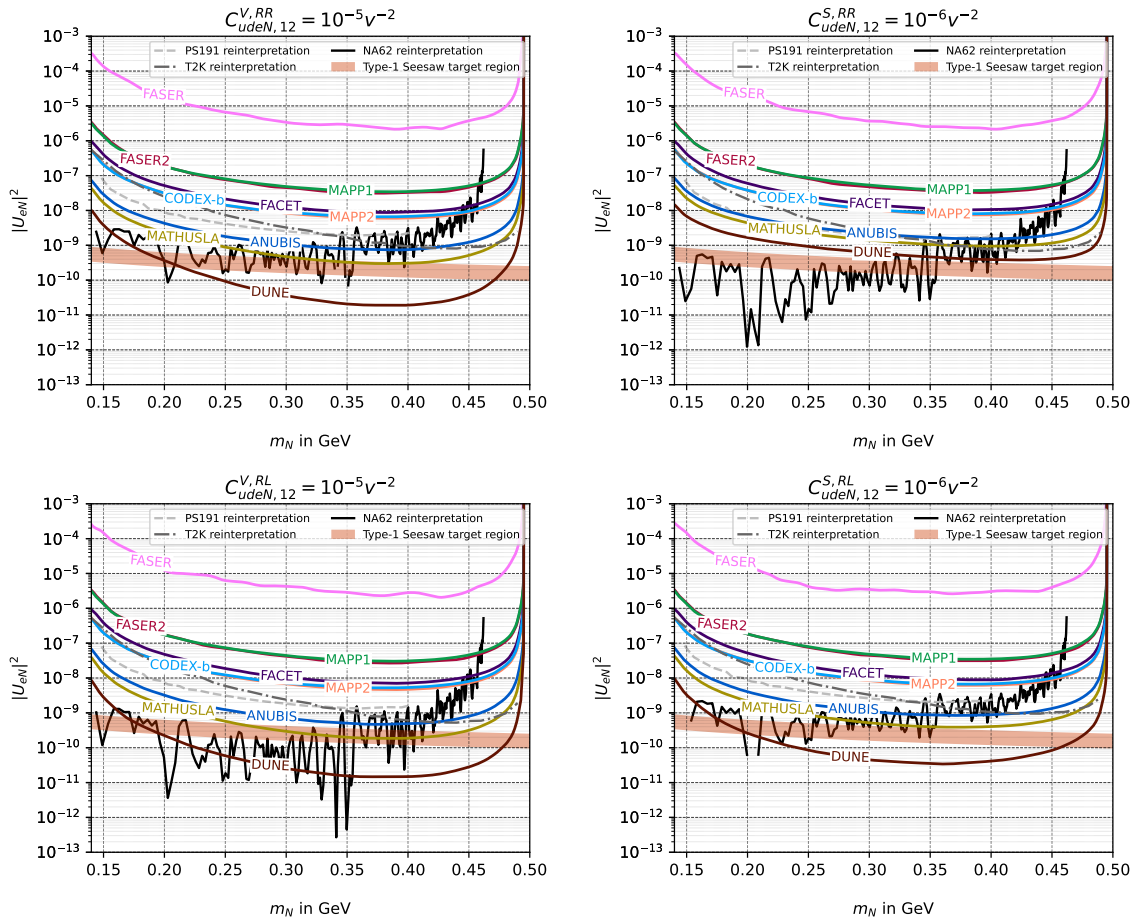


**Figure 7.** Projected exclusion limits in the plane  $|U_{eN}|^2$  vs.  $m_N$  for single- $N_R$  operator benchmarks B5 and B6 (top), and B7 and B8 (bottom). The absolute value of the corresponding WC has been fixed to  $10^{-5}v^{-2}$  and  $10^{-6}v^{-2}$  for vector and scalar operators, respectively. The recast bounds from NA62, T2K, and PS191 are also shown.

type) operators. On the other hand, the DUNE-ND can exclude new parameter space for  $m_N \gtrsim 0.25$  (0.35) GeV in benchmarks B5, B7, and B8 (B6), showing again the much better constraining power than the future LLP far detectors. In the plots for the benchmarks B5, B7, and B8, we observe a unique funnel feature in the DUNE sensitivity reach for  $m_N$  roughly between 0.36 GeV and 0.4 GeV. This arises from the fact that in this mass range with  $|U_{eN}|^2 = 10^{-10}$ , even in the absence of the effective operators considered, more than three signal events are predicted at DUNE (see figure 6 of Ref. [33]),<sup>9</sup> as long as the interference between the minimal mixing and the EFT operators for the HNL production is constructive. Indeed, the funnel feature of the DUNE sensitivities do not appear in B6 (the upper right plot), exactly as a result of the destructive interference in this case. To illustrate

<sup>9</sup>We stress that the apparent sensitivity at small values of the operator coefficients is feigned. There is no real sensitivity to such small coefficients, since the event number does not depend on the operator anymore.

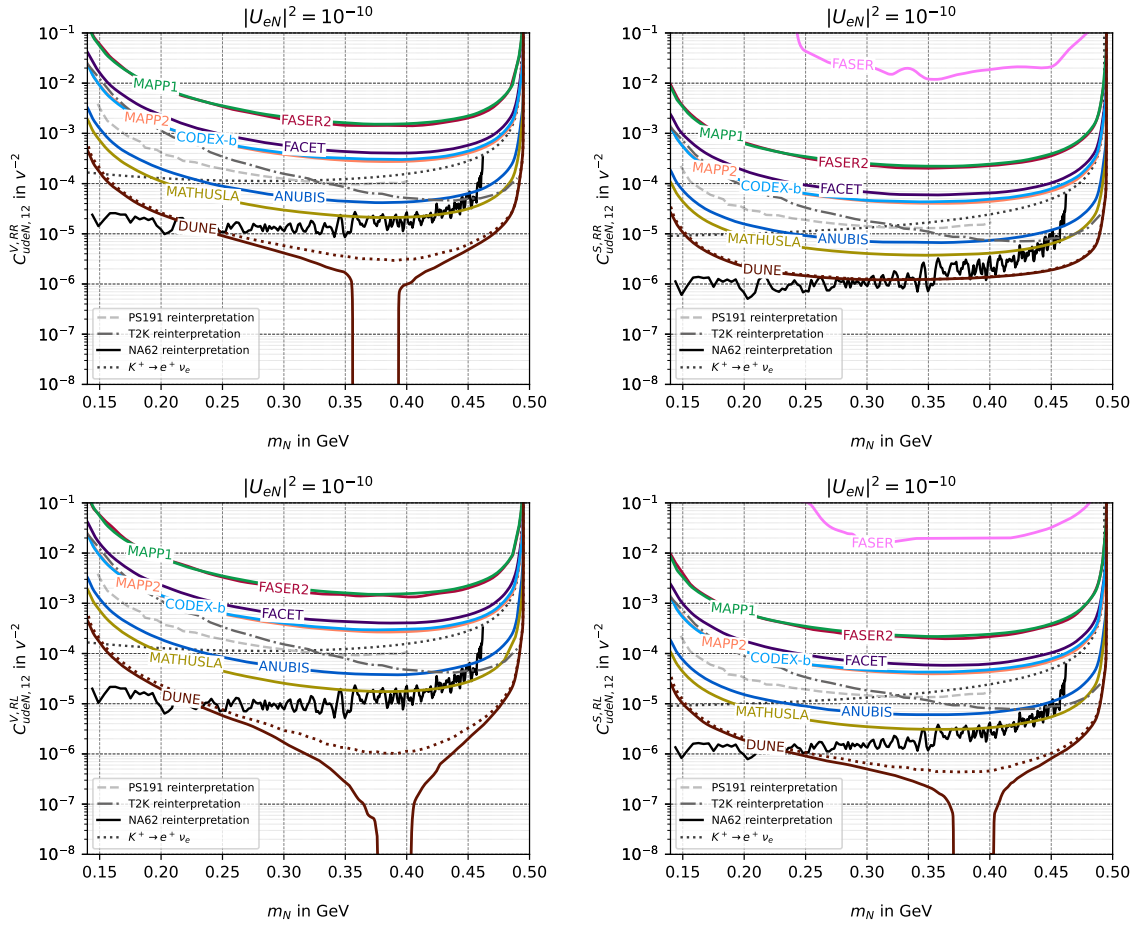


**Figure 8.** Exclusion limits in the plane WC vs.  $m_N$  for single- $N_R$  operator benchmarks B5 and B6 (top), and B7 and B8 (bottom). The active-heavy neutrino mixing parameter has been fixed as  $|U_{eN}|^2 = 10^{-10}$ . The recast bounds from NA62, T2K, and PS191, as well as the constraint originating from the measured branching ratio of  $K^+ \rightarrow e^+ \nu_e$ , are also shown. For the predictions on the sensitivities of DUNE (brown), we show an extra curve in dotted line style corresponding to  $|U_{eN}|^2 = 8 \times 10^{-11}$ .

this effect better, we choose to show, in all these four plots, an additional sensitivity curve for DUNE corresponding to  $|U_{eN}|^2 = 8 \times 10^{-11}$  which is slightly smaller than the default  $10^{-10}$  value we have chosen. We now observe that the funnel feature in B5, B7, and B8 has disappeared, and in the plot for B6, we find the two DUNE curves for  $|U_{eN}|^2 = 10^{-10}$  and  $8 \times 10^{-11}$  almost completely overlap as a result of the two values' closeness. We further see, that the NA62 constraints for B6 and B8 exclude  $WC \gtrsim 10^{-6} v^{-2}$ , justifying the WC choice in figure 7. Overall, for benchmarks B5–B8, the future far detectors will access new parameter space for larger HNL masses, while DUNE shows much more promising sensitivities even for  $m_N$  as low as 0.25 GeV.

## 5 Summary

In this work, we have studied the potential of present and future far-detector experiments at the LHC and the beam-dump-type experiment DUNE, for probing long-lived heavy neutral leptons (HNLs) of Majorana nature produced from rare kaon decays, in the theoretical framework of low-energy effective field theory extended with sterile neutrinos ( $N_{R\text{LEFT}}$ ). We have focused on dimension-6 effective operators consisting of a pair of quarks together with a charged lepton and an HNL, or a pair of HNLs. Besides the effective operators, we also take into account the minimal mixing parameter between the HNLs and the standard-model active neutrinos. For simplicity, we assume in this work that there is only one kinematically relevant HNL, that the HNL mixes with the electron neutrino only, and that for the effective operators also only the first-generation leptons are considered.

There are both lepton-number-conserving and lepton-number-violating operators; we have investigated both of them and elaborated on their differences. We have computed the kaons' decay branching ratios into the HNLs with the considered effective operators, as a function of the HNL mass, the effective couplings, and the mixing parameter  $U_{eN}$ . In addition, the decay rates of the HNLs in the  $N_{R\text{LEFT}}$  are calculated with care, including the interference between the EFT operators and the minimal mixing contributions. We have further performed detailed Monte-Carlo simulations, in order to determine the acceptance of the LHC far detectors and the DUNE-ND for the long-lived HNLs. The LHC experiments include ANUBIS, CODEX-b, FASER and FASER2, FACET, MATHUSLA, and MoeDAL-MAPP1 and MAPP2. In particular, because of the long-lifetime nature of the kaons ( $K^\pm$ ,  $K_S$ , and  $K_L$ ), we cannot assume they decay essentially at the IPs; we have thus taken into account their decay positions in the simulation when we compute the decay probability of the HNLs in the detector fiducial volumes. Moreover, for the various experiments, we have properly placed a cut-off position for each LHC far detector beyond which the kaons are vetoed.

For a series of benchmark scenarios classified by the number of HNLs in the operators as well as the Lorentz structure of the operators, we have obtained numerical results. Besides the projection for the considered experiments, we have recast existing bounds on the HNLs in the minimal mixing scenario into those on the HNLs in the considered EFT benchmarks. We find that for the pair- $N_R$  scenarios, the existing bounds from NA62 are already so strong that it has excluded all the parameter space that could be probed by future LHC far-detector experiments, but DUNE can still be sensitive to new parameter space in the case of scalar-type operators (benchmarks B2.1 and B2.2). On the other hand, for the single- $N_R$  benchmarks, the studied future experiments are sensitive to regions of parameter space currently unexcluded. Particularly, for benchmarks B3 and B4, the projected limits on the effective couplings can be orders of magnitude stronger than the existing bounds. In all these benchmarks, we find the projected sensitivities for DUNE-ND are stronger than those for the LHC far detectors by various degrees in different benchmarks, mainly in virtue of the much larger production rates of the kaons at DUNE.

To summarize, our findings in this work show that for long-lived HNLs in the EFT framework produced from kaons, the DUNE-ND is expected to have sensitivities much more promising than the present and future LHC far detectors. Nevertheless, the LHC far detectors can probe unexcluded parameter space in some scenarios, motivating their construction and operation during the HL phase of the LHC.

## Acknowledgements

We thank Juan Carlos Helo and Felix Kling for useful discussions, and thank Giovanna Cottin for contributions in the early stage of the project. This work is supported by the Spanish grants PID2020-113775GB-I00 (AEI/10.13039/501100011033) and CIPROM/2021/054 (Generalitat Valenciana). R.B. acknowledges financial support from the Generalitat Valenciana (grant ACIF/2021/052).

## A Kaon decays into HNLs

Throughout this work, we assume  $N$  to be a Majorana particle. We neglect  $|\varepsilon| \ll 1$  responsible for indirect  $CP$  violation in the neutral kaon system, such that  $K_S$  and  $K_L$  coincide with  $K_1$  and  $K_2$  given by eq. (2.2). Since the latter are superpositions of flavor eigenstates and the effective operators we consider are written in the flavor basis, it proves convenient to define the following combinations of the Wilson coefficients:

$$a_{ij}^V \equiv c_{dN,ij}^{V,RR} - c_{dN,ij}^{V,LR} \quad \text{and} \quad a_{ij}^S \equiv c_{dN,ij}^{S,RR} - c_{dN,ij}^{S,LR}, \quad (\text{A.1})$$

$$b_{ij}^V \equiv c_{dN,ij}^{V,RR} + c_{dN,ij}^{V,LR} \quad \text{and} \quad b_{ij}^S \equiv c_{dN,ij}^{S,RR} + c_{dN,ij}^{S,LR}. \quad (\text{A.2})$$

In addition, for the single- $N_R$  operators with a charged lepton, we define

$$c_{ij}^V \equiv c_{udeN,ij}^{V,RR} - c_{udeN,ij}^{V,LR} \quad \text{and} \quad c_{ij}^S \equiv c_{udeN,ij}^{S,RR} - c_{udeN,ij}^{S,LR}, \quad (\text{A.3})$$

$$d_{ij}^V \equiv c_{udeN,ij}^{V,RL} - c_{udeN,ij}^{V,LL} \quad \text{and} \quad d_{ij}^S \equiv c_{udeN,ij}^{S,RL} - c_{udeN,ij}^{S,LL}, \quad (\text{A.4})$$

$$g_{ij}^V \equiv c_{udeN,ij}^{V,RR} + c_{udeN,ij}^{V,LR} \quad \text{and} \quad g_{ij}^S \equiv c_{udeN,ij}^{S,RR} + c_{udeN,ij}^{S,LR}, \quad (\text{A.5})$$

$$h_{ij}^V \equiv c_{udeN,ij}^{V,RL} + c_{udeN,ij}^{V,LL} \quad \text{and} \quad h_{ij}^S \equiv c_{udeN,ij}^{S,RL} + c_{udeN,ij}^{S,LL}. \quad (\text{A.6})$$

### A.1 Form factors

The non-zero hadronic matrix elements entering the computations of kaon decay amplitudes are given by

$$\langle 0 | \bar{s} \gamma^\mu \gamma_5 d | K^0 \rangle = i f_K p_K^\mu, \quad (\text{A.7})$$

$$\langle 0 | \bar{s} \gamma_5 d | K^0 \rangle = i \frac{m_K^2}{m_d + m_s} f_K \equiv i f_K^S, \quad (\text{A.8})$$

for leptonic kaon decays. Here  $m_K = 493.6$  MeV is the neutral kaon mass, and  $f_K = 155.7$  MeV [68], and  $f_K^S$  are the kaon decay constants. For  $K^0 \rightarrow \pi^-$  transitions, the

Parameter	$f_+(0)$	$\Lambda_+$	$\log C$	$G(0)$	$B_T(0)/f_+(0)$	$s_T^{K\pi}$ [GeV <sup>-2</sup> ]
Central value	0.9706	0.02422	0.1198	0.0398	0.68	1.10

**Table 5.** Parameters entering the form factors  $f_+$ ,  $f_0$  and  $B_T$  in eqs. (A.12)–(A.14).

relevant matrix elements read

$$\langle \pi^- | \bar{s} \gamma^\mu u | K^0 \rangle = f_+(q^2) P^\mu + (f_0(q^2) - f_+(q^2)) \frac{m_K^2 - m_\pi^2}{q^2} q^\mu, \quad (\text{A.9})$$

$$\langle \pi^- | \bar{s} u | K^0 \rangle = \frac{m_K^2 - m_\pi^2}{m_u - m_s} f_0(q^2) \equiv f_S(q^2), \quad (\text{A.10})$$

$$\langle \pi^- | \bar{s} \sigma^{\mu\nu} u | K^0 \rangle = \frac{i}{m_K} (p_K^\mu p_\pi^\nu - p_K^\nu p_\pi^\mu) B_T(q^2), \quad (\text{A.11})$$

where  $P = p_K + p_\pi$  is the sum of the kaon and pion 4-momenta, and  $q = p_K - p_\pi$  is their difference. The three form factors ( $f_+$ ,  $f_0$ ,  $B_T$ ) can be parameterized in terms of  $q^2$  as follows (see Ref. [69] for more detail)

$$f_+(q^2) = f_+(0) + \Lambda_+ \frac{q^2}{m_\pi^2}, \quad (\text{A.12})$$

$$f_0(q^2) = f_+(0) + (\log C - G(0)) \frac{m_\pi^2}{m_K^2 - m_\pi^2} \frac{q^2}{m_\pi^2}, \quad (\text{A.13})$$

$$B_T(q^2) = B_T(0) (1 - s_T^{K\pi} q^2), \quad (\text{A.14})$$

and the numerical values of the parameters entering these expressions are reported in table 5.

## A.2 Two-body decays

The partial decay widths of  $K_{S/L} \rightarrow NN$  mediated by the pair- $N_R$  operators  $\mathcal{O}_{dN}$  given in table 1 read:

$$\begin{aligned} \Gamma(K_S \rightarrow NN) &= \frac{m_K}{32\pi} \sqrt{1 - \frac{4m_N^2}{m_K^2}} \left[ 4f_K^2 m_N^2 (\text{Im } a_{21}^V)^2 \right. \\ &\quad \left. + (f_K^S)^2 \left\{ [\text{Im}(a_{21}^S - a_{12}^S)]^2 + [\text{Re}(a_{21}^S - a_{12}^S)]^2 \left(1 - \frac{4m_N^2}{m_K^2}\right) \right\} \right. \\ &\quad \left. + 4f_K f_K^S m_N \text{Im } a_{21}^V \text{Im}(a_{21}^S - a_{12}^S) \right], \quad (\text{A.15}) \end{aligned}$$

$$\begin{aligned} \Gamma(K_L \rightarrow NN) &= \frac{m_K}{32\pi} \sqrt{1 - \frac{4m_N^2}{m_K^2}} \left[ 4f_K^2 m_N^2 (\text{Re } a_{21}^V)^2 \right. \\ &\quad \left. + (f_K^S)^2 \left\{ [\text{Re}(a_{21}^S + a_{12}^S)]^2 + [\text{Im}(a_{21}^S + a_{12}^S)]^2 \left(1 - \frac{4m_N^2}{m_K^2}\right) \right\} \right. \\ &\quad \left. + 4f_K f_K^S m_N \text{Re } a_{21}^V \text{Re}(a_{21}^S + a_{12}^S) \right]. \quad (\text{A.16}) \end{aligned}$$

In this computation, we have neglected the contribution from active-heavy mixing for two reasons: (i) the amplitude for  $K_{S/L} \rightarrow NN$  is proportional to  $U_{\ell N}^2$  and  $|U_{\ell N}|^2 \ll 1$ , and (ii) flavor-changing neutral currents are further suppressed, since in the SM they do not occur at tree level.

The single- $N_R$  operators with a charged lepton summarized in table 2 as well as the standard active-heavy neutrino mixing trigger  $K^- \rightarrow \ell^- N$ . For the corresponding decay width, we find

$$\begin{aligned} \Gamma(K^- \rightarrow \ell^- N) = & \frac{\lambda^{1/2}(m_K^2, m_\ell^2, m_N^2)}{64\pi m_K^3} \left\{ f_K^2 \left( |c_{12}^V|^2 + |d_{12}^V|^2 + |c_{\text{mix}}|^2 - 2 \text{Re}(d_{12}^V c_{\text{mix}}^*) \right) \right. \\ & \times \left[ m_K^2 (m_\ell^2 + m_N^2) - (m_\ell^2 - m_N^2)^2 \right] \\ & + (f_K^S)^2 \left( |c_{12}^S|^2 + |d_{12}^S|^2 \right) [m_K^2 - m_\ell^2 - m_N^2] \\ & + 2f_K f_K^S \text{Re}(c_{12}^V c_{12}^{S*} + d_{12}^V d_{12}^{S*} - d_{12}^{S*} c_{\text{mix}}) m_\ell [m_K^2 - m_\ell^2 + m_N^2] \\ & - 4f_K^2 \text{Re}(c_{12}^V d_{12}^{V*} - c_{12}^V c_{\text{mix}}^*) m_K^2 m_\ell m_N - 4(f_K^S)^2 \text{Re}(c_{12}^S d_{12}^{S*}) m_\ell m_N \\ & \left. - 2f_K f_K^S \text{Re}(c_{12}^V d_{12}^{S*} + c_{12}^S d_{12}^{V*} - c_{12}^S c_{\text{mix}}^*) m_N [m_K^2 + m_\ell^2 - m_N^2] \right\}, \quad (\text{A.17}) \end{aligned}$$

where  $\lambda(x, y, z) = x^2 + y^2 + z^2 - 2xy - 2xz - 2yz$ . This result complements eq. (52) of Ref. [29], where only one LNV operator ( $C_{\text{VLL}}^{(6)}$  in their notation) arising from the  $N_R$ SMEFT at  $d = 6$  has been included. In our notation, it means  $d_{12}^V = -c_{udeN,12}^{V,LL}$  and  $d_{12}^S = 0$ . We find agreement with eq. (52) of Ref. [29] in this limit.

### A.3 Three-body decays

We rely on the isospin symmetry and express the results in terms of the form factors  $f_+$ ,  $f_0$ ,  $f_S$  and  $B_T$  for  $\langle \pi^- | \bar{s} \Gamma u | K^0 \rangle$  given in eqs. (A.12)–(A.14). By the isospin symmetry, we have

$$\langle \pi^0 | \bar{s} \Gamma d | K^0 \rangle = -\frac{1}{\sqrt{2}} \langle \pi^- | \bar{s} \Gamma u | K^0 \rangle, \quad (\text{A.18})$$

$$\langle \pi^+ | \bar{s} \Gamma d | K^+ \rangle = \langle \pi^- | \bar{s} \Gamma u | K^0 \rangle. \quad (\text{A.19})$$

The amplitude for  $K_{S/L} \rightarrow \pi^0 NN$  is given by

$$\begin{aligned} \mathcal{M}(K_{S/L} \rightarrow \pi^0 NN) = & \frac{1}{4} (b_{21}^V \pm b_{21}^{V*}) \left[ f_+ P_\mu + (f_0 - f_+) \frac{m_K^2 - m_\pi^2}{q^2} q_\mu \right] [\bar{u}_N \gamma^\mu \gamma_5 v_{N'}] \\ & + \frac{f_S}{2} (b_{21}^S \mp b_{12}^S) [\bar{u}_N P_R v_{N'}] + \frac{f_S}{2} (b_{12}^S \mp b_{21}^S)^* [\bar{u}_N P_L v_{N'}]. \quad (\text{A.20}) \end{aligned}$$

The squared amplitudes summed over spins then read:

$$\begin{aligned} \sum_{\text{spins}} |\mathcal{M}(K_S \rightarrow \pi^0 NN)|^2 = & 2 (\text{Re } b_{21}^V)^2 \left\{ -4f_+^2 (p \cdot p_N)^2 + 2f_+^2 (a + m_K^2 - m_\pi^2) (p \cdot p_N) \right. \\ & \left. - f_+^2 [a(m_K^2 + m_N^2) - 2m_N^2(m_K^2 + m_\pi^2)] + \frac{(f_0^2 - f_+^2)}{a} m_N^2 (m_K^2 - m_\pi^2)^2 \right\} \end{aligned}$$

$$\begin{aligned}
& + \frac{f_S^2}{2} \left\{ [\text{Re}(b_{21}^S - b_{12}^S)]^2 a + [\text{Im}(b_{21}^S - b_{12}^S)]^2 (a - 4m_N^2) \right\} \\
& + 2f_0 f_S m_N (m_K^2 - m_\pi^2) \text{Re} b_{21}^V \text{Re}(b_{21}^S - b_{12}^S), \tag{A.21}
\end{aligned}$$

$$\begin{aligned}
\sum_{\text{spins}} |\mathcal{M}(K_L \rightarrow \pi^0 NN)|^2 &= 2 (\text{Im} b_{21}^V)^2 \left\{ -4f_+^2 (p \cdot p_N)^2 + 2f_+^2 (a + m_K^2 - m_\pi^2) (p \cdot p_N) \right. \\
& - f_+^2 [a(m_K^2 + m_N^2) - 2m_N^2(m_K^2 + m_\pi^2)] + \frac{(f_0^2 - f_+^2)}{a} m_N^2 (m_K^2 - m_\pi^2)^2 \left. \right\} \\
& + \frac{f_S^2}{2} \left\{ [\text{Im}(b_{21}^S + b_{12}^S)]^2 a + [\text{Re}(b_{21}^S + b_{12}^S)]^2 (a - 4m_N^2) \right\} \\
& + 2f_0 f_S m_N (m_K^2 - m_\pi^2) \text{Im} b_{21}^V \text{Im}(b_{21}^S + b_{12}^S). \tag{A.22}
\end{aligned}$$

For  $K^+ \rightarrow \pi^+ NN$ , we find:

$$\begin{aligned}
\mathcal{M}(K^+ \rightarrow \pi^+ NN) &= \frac{b_{21}^V}{2} \left[ f_+ P_\mu + (f_0 - f_+) \frac{M^2 - m^2}{q^2} q_\mu \right] [\bar{u}_N \gamma^\mu \gamma_5 v_{N'}] \\
& + f_S b_{21}^S [\bar{u}_N P_R v_{N'}] + f_S b_{12}^{S*} [\bar{u}_N P_L v_{N'}], \tag{A.23}
\end{aligned}$$

and

$$\begin{aligned}
\sum_{\text{spins}} |\mathcal{M}(K^+ \rightarrow \pi^+ NN)|^2 &= 2 |b_{21}^V|^2 \left\{ -4f_+^2 (p \cdot p_N)^2 + 2f_+^2 (a + m_K^2 - m_\pi^2) (p \cdot p_N) \right. \\
& - f_+^2 [a(m_K^2 + m_N^2) - 2m_N^2(m_K^2 + m_\pi^2)] + \frac{(f_0^2 - f_+^2)}{a} m_N^2 (m_K^2 - m_\pi^2)^2 \left. \right\} \\
& + f_S^2 \left\{ (|b_{21}^S|^2 + |b_{12}^S|^2) (a - 2m_N^2) - 4m_N^2 \text{Re}(b_{21}^S b_{12}^S) \right\} \\
& + 2f_0 f_S m_N (m_K^2 - m_\pi^2) \text{Re} [b_{21}^V (b_{21}^{S*} - b_{12}^S)]. \tag{A.24}
\end{aligned}$$

Turning to the single- $N_R$  operators with a charged lepton, we have

$$\begin{aligned}
\mathcal{M}(K^- \rightarrow \pi^0 \ell^- N) &= \frac{1}{2\sqrt{2}} \left\{ g_{12}^V [\bar{u}_\ell \gamma^\mu P_R v_N] + (h_{12}^V + c_{\text{mix}}) [\bar{u}_\ell \gamma^\mu P_L v_N] \right\} \\
& \times \left[ f_+ P_\mu + (f_0 - f_+) \frac{m_K^2 - m_\pi^2}{q^2} q_\mu \right] \\
& + \frac{f_S}{2\sqrt{2}} \left\{ g_{12}^S [\bar{u}_\ell P_R v_N] + h_{12}^S [\bar{u}_\ell P_L v_N] \right\} \\
& + \frac{i}{2\sqrt{2}} \frac{B_T}{m_K} \left\{ [p^\mu p'^\nu - p^\nu p'^\mu + i \epsilon_{\mu\nu\alpha\beta} p^\alpha p'^\beta] c_{udeN,12}^{T,RR} [\bar{u}_\ell \sigma^{\mu\nu} P_R v_N] \right. \\
& \left. + [p^\mu p'^\nu - p^\nu p'^\mu - i \epsilon_{\mu\nu\alpha\beta} p^\alpha p'^\beta] c_{udeN,12}^{T,LL} [\bar{u}_\ell \sigma^{\mu\nu} P_L v_N] \right\}. \tag{A.25}
\end{aligned}$$

Finally, up to an unphysical sign,

$$\mathcal{M}(K_{S/L} \rightarrow \pi^+ \ell^- N) = \mathcal{M}(K^- \rightarrow \pi^0 \ell^- N). \tag{A.26}$$



We do not provide the full expression for the modulus square of amplitude (A.25) summed over spins, since it is rather cumbersome. However, it is straightforward to obtain it, especially, assuming only one operator (either V, S, or T) at a time. In the limit of zero mixing ( $c_{\text{mix}} = 0$ ), as in the case of two-body decay in eq. (A.17), the LNV single- $N_R$  operators (switched on one at a time) lead to the same results as their LNC counterparts. Finally, the three-body decay widths are computed following the procedure explained in Refs. [29, 30].

## B HNL decays

Effective operators in  $N_R\text{LEFT}$  not only enhance the HNL production but also trigger their decay. Assuming only one generation of  $N_R$ , the pair- $N_R$  operators in table 1 cannot make the HNL decay, whereas the single- $N_R$  operators in table 2 do contribute to it. In this appendix we provide the partial decay width of  $N \rightarrow \ell^- \pi^+$ , which is the only kinematically allowed channel if HNLs are produced in kaon decays and if  $m_N > m_\pi + m_\ell$ . In the computation we take into account the contribution from (i) the  $\mathcal{O}_{udeN}$  operators in table 2, (ii) eq. (2.4), *i.e.* the standard mixing to active neutrinos, and (iii) the interference terms between (i) and (ii). The final expression reads

$$\begin{aligned} \Gamma(N \rightarrow \ell^- \pi^+) = & \frac{\lambda^{1/2} (m_N^2, m_\ell^2, m_\pi^2)}{128\pi m_N^3} \left\{ f_\pi^2 \left( |c_{11}^V|^2 + |d_{11}^V|^2 + |c_{\text{mix}}|^2 - 2 \text{Re} (d_{11}^V c_{\text{mix}}^*) \right) \right. \\ & \times \left[ (m_\ell^2 - m_N^2)^2 - m_\pi^2 (m_\ell^2 + m_N^2) \right] \\ & + (f_\pi^S)^2 \left( |c_{11}^S|^2 + |d_{11}^S|^2 \right) [m_\ell^2 + m_N^2 - m_\pi^2] \\ & - 2f_\pi f_\pi^S \text{Re} (c_{11}^V c_{11}^{S*} + d_{11}^V d_{11}^{S*} - c_{\text{mix}} d_{11}^{S*}) m_\ell [m_\ell^2 - m_N^2 - m_\pi^2] \\ & + 4f_\pi^2 \text{Re} (c_{11}^V d_{11}^{V*} - c_{11}^V c_{\text{mix}}^*) m_\pi^2 m_\ell m_N + 4 (f_\pi^S)^2 \text{Re} (c_{11}^S d_{11}^{S*}) m_\ell m_N \\ & \left. - 2f_\pi f_\pi^S \text{Re} (c_{11}^V d_{11}^{S*} + c_{11}^S d_{11}^{V*} - c_{11}^S c_{\text{mix}}^*) m_N [m_\ell^2 - m_N^2 + m_\pi^2] \right\}. \quad (\text{B.1}) \end{aligned}$$

The previous result can be derived from the amplitude leading to eq. (A.17) by substituting  $K$  with  $\pi$  and performing the interchange  $p_\pi \leftrightarrow p_N$  along the computation. The decay constants are given by  $f_\pi = 130.2 \text{ MeV}$  [68] and  $f_\pi^S = \frac{m_\pi^2}{m_u + m_d} f_\pi$ . We have also used the notation introduced in appendix A for the WC, and  $c_{\text{mix}}$  is the coefficient defined in eq. (2.5).

In the scenarios outlined in table 4, the decay of the HNL is governed by either the neutrino mixing parameter (scenarios B1–B2 and B5–B8) or one of the WC of the effective operators (scenarios B3 and B4). In cases where the former applies, eq. (B.1) reduces to the one in the minimal scenario [70]. Conversely, in the latter cases, eq. (B.1) can be simplified to

$$\Gamma(N \rightarrow \ell^- \pi^+) = \frac{\lambda^{1/2} (m_N^2, m_\ell^2, m_\pi^2)}{128\pi m_N^3} \left\{ f_\pi^2 \left( |c_{11}^V|^2 + |d_{11}^V|^2 \right) \left[ (m_\ell^2 - m_N^2)^2 - m_\pi^2 (m_\ell^2 + m_N^2) \right] \right\}$$

$$\begin{aligned}
& + (f_\pi^S)^2 \left( |c_{11}^S|^2 + |d_{11}^S|^2 \right) [m_\ell^2 + m_N^2 - m_\pi^2] \\
& + 4f_\pi^2 \operatorname{Re} (c_{11}^V d_{11}^{V*}) m_\pi^2 m_\ell m_N + 4 (f_\pi^S)^2 \operatorname{Re} (c_{11}^S d_{11}^{S*}) m_\ell m_N \\
& - 2f_\pi f_\pi^S \operatorname{Re} (c_{11}^V c_{11}^{S*} + d_{11}^V d_{11}^{S*}) m_\ell [m_\ell^2 - m_N^2 - m_\pi^2] \\
& - 2f_\pi f_\pi^S \operatorname{Re} (c_{11}^V d_{11}^{S*} + c_{11}^S d_{11}^{V*}) m_N [m_\ell^2 - m_N^2 + m_\pi^2] \Big\}. \tag{B.2}
\end{aligned}$$

It is worth mentioning that in scenarios B1–B2 and B5–B8, there are additional decay channels for  $N$ , such as the purely leptonic  $\nu\nu\nu$  and  $\nu\ell\ell$  channels, which enhance the HNL total decay width. The possible open channels depend on the HNL mass [70]. Meanwhile, in scenarios B3–B4, the total decay width becomes twice the result in eq. (B.2), since the charge conjugated channel is also open for Majorana  $N$ .

## References

- [1] D. Curtin et al., *Long-Lived Particles at the Energy Frontier: The MATHUSLA Physics Case*, *Rept. Prog. Phys.* **82** (2019) 116201 [1806.07396].
- [2] J. Alimena et al., *Searching for long-lived particles beyond the Standard Model at the Large Hadron Collider*, *J. Phys. G* **47** (2020) 090501 [1903.04497].
- [3] J.L. Feng et al., *The Forward Physics Facility at the High-Luminosity LHC*, *J. Phys. G* **50** (2023) 030501 [2203.05090].
- [4] J.L. Feng, I. Galon, F. Kling and S. Trojanowski, *ForwArd Search ExpeRiment at the LHC*, *Phys. Rev. D* **97** (2018) 035001 [1708.09389].
- [5] FASER collaboration, *FASER’s physics reach for long-lived particles*, *Phys. Rev. D* **99** (2019) 095011 [1811.12522].
- [6] J.L. Pinfold, *The MoEDAL Experiment at the LHC—A Progress Report*, *Universe* **5** (2019) 47.
- [7] J.L. Pinfold, *The MoEDAL experiment: a new light on the high-energy frontier*, *Phil. Trans. Roy. Soc. Lond. A* **377** (2019) 20190382.
- [8] M. Bauer, O. Brandt, L. Lee and C. Ohm, *ANUBIS: Proposal to search for long-lived neutral particles in CERN service shafts*, [1909.13022](#).
- [9] V.V. Gligorov, S. Knapen, M. Papucci and D.J. Robinson, *Searching for Long-lived Particles: A Compact Detector for Exotics at LHCb*, *Phys. Rev. D* **97** (2018) 015023 [1708.09395].
- [10] S. Cerci et al., *FACET: A new long-lived particle detector in the very forward region of the CMS experiment*, *JHEP* **2022** (2022) 110 [2201.00019].
- [11] J.P. Chou, D. Curtin and H.J. Lubatti, *New Detectors to Explore the Lifetime Frontier*, *Phys. Lett. B* **767** (2017) 29 [1606.06298].
- [12] MATHUSLA collaboration, *An Update to the Letter of Intent for MATHUSLA: Search for Long-Lived Particles at the HL-LHC*, [2009.01693](#).
- [13] DUNE collaboration, *Deep Underground Neutrino Experiment (DUNE), Far Detector Technical Design Report, Volume I Introduction to DUNE*, *JINST* **15** (2020) T08008 [2002.02967].

- [14] DUNE collaboration, *Deep Underground Neutrino Experiment (DUNE), Far Detector Technical Design Report, Volume II: DUNE Physics*, 2002.03005.
- [15] DUNE collaboration, *Long-baseline neutrino oscillation physics potential of the DUNE experiment*, *Eur. Phys. J. C* **80** (2020) 978 [2006.16043].
- [16] DUNE collaboration, *Experiment Simulation Configurations Approximating DUNE TDR*, 2103.04797.
- [17] DUNE collaboration, *Low exposure long-baseline neutrino oscillation sensitivity of the DUNE experiment*, *Phys. Rev. D* **105** (2022) 072006 [2109.01304].
- [18] DUNE collaboration, *Deep Underground Neutrino Experiment (DUNE) Near Detector Conceptual Design Report*, *Instruments* **5** (2021) 31 [2103.13910].
- [19] C. Antel et al., *Feebly Interacting Particles: FIPs 2022 workshop report*, in *Workshop on Feebly-Interacting Particles*, 5, 2023 [2305.01715].
- [20] F. del Aguila, S. Bar-Shalom, A. Soni and J. Wudka, *Heavy Majorana Neutrinos in the Effective Lagrangian Description: Application to Hadron Colliders*, *Phys. Lett. B* **670** (2009) 399 [0806.0876].
- [21] A. Aparici, K. Kim, A. Santamaria and J. Wudka, *Right-handed neutrino magnetic moments*, *Phys. Rev. D* **80** (2009) 013010 [0904.3244].
- [22] S. Bhattacharya and J. Wudka, *Dimension-seven operators in the standard model with right handed neutrinos*, *Phys. Rev. D* **94** (2016) 055022 [1505.05264].
- [23] Y. Liao and X.-D. Ma, *Operators up to Dimension Seven in Standard Model Effective Field Theory Extended with Sterile Neutrinos*, *Phys. Rev. D* **96** (2017) 015012 [1612.04527].
- [24] R. Beltrán, R. Cepedello and M. Hirsch, *Tree-level UV completions for  $N_R$  SMEFT  $d = 6$  and  $d = 7$  operators*, *JHEP* **08** (2023) 166 [2306.12578].
- [25] G. Cottin, J.C. Helo, M. Hirsch, A. Titov and Z.S. Wang, *Heavy neutral leptons in effective field theory and the high-luminosity LHC*, *JHEP* **09** (2021) 039 [2105.13851].
- [26] R. Beltrán, G. Cottin, J.C. Helo, M. Hirsch, A. Titov and Z.S. Wang, *Long-lived heavy neutral leptons at the LHC: four-fermion single- $N_R$  operators*, *JHEP* **01** (2022) 044 [2110.15096].
- [27] W. Liu and Y. Zhang, *Testing neutrino dipole portal by long-lived particle detectors at the LHC*, *Eur. Phys. J. C* **83** (2023) 568 [2302.02081].
- [28] F. Delgado, L. Duarte, J. Jones-Perez, C. Manrique-Chavil and S. Peña, *Assessment of the dimension-5 seesaw portal and impact of exotic Higgs decays on non-pointing photon searches*, *JHEP* **09** (2022) 079 [2205.13550].
- [29] J. De Vries, H.K. Dreiner, J.Y. Günther, Z.S. Wang and G. Zhou, *Long-lived Sterile Neutrinos at the LHC in Effective Field Theory*, *JHEP* **03** (2021) 148 [2010.07305].
- [30] R. Beltrán, G. Cottin, J.C. Helo, M. Hirsch, A. Titov and Z.S. Wang, *Long-lived heavy neutral leptons from mesons in effective field theory*, *JHEP* **01** (2023) 015 [2210.02461].
- [31] D. Barducci, E. Bertuzzo, M. Taoso and C. Toni, *Probing right-handed neutrinos dipole operators*, *JHEP* **03** (2023) 239 [2209.13469].

- [32] D. Barducci, W. Liu, A. Titov, Z.S. Wang and Y. Zhang, *Probing the dipole portal to heavy neutral leptons via meson decays at the high-luminosity LHC*, [2308.16608](#).
- [33] J.Y. Günther, J. de Vries, H.K. Dreiner, Z.S. Wang and G. Zhou, *Long-lived neutral fermions at the DUNE near detector*, *JHEP* **01** (2024) 108 [[2310.12392](#)].
- [34] I. Bischer and W. Rodejohann, *General neutrino interactions from an effective field theory perspective*, *Nucl. Phys. B* **947** (2019) 114746 [[1905.08699](#)].
- [35] M. Chala and A. Titov, *One-loop matching in the SMEFT extended with a sterile neutrino*, *JHEP* **05** (2020) 139 [[2001.07732](#)].
- [36] T. Li, X.-D. Ma and M.A. Schmidt, *General neutrino interactions with sterile neutrinos in light of coherent neutrino-nucleus scattering and meson invisible decays*, *JHEP* **07** (2020) 152 [[2005.01543](#)].
- [37] T. Li, X.-D. Ma and M.A. Schmidt, *Constraints on the charged currents in general neutrino interactions with sterile neutrinos*, *JHEP* **10** (2020) 115 [[2007.15408](#)].
- [38] G. Zhou, J.Y. Günther, Z.S. Wang, J. de Vries and H.K. Dreiner, *Long-lived sterile neutrinos at Belle II in effective field theory*, *JHEP* **04** (2022) 057 [[2111.04403](#)].
- [39] T. Han, J. Liao, H. Liu and D. Marfatia, *Right-handed Dirac and Majorana neutrinos at Belle II*, *JHEP* **04** (2023) 013 [[2207.07029](#)].
- [40] SHiP collaboration, *A facility to Search for Hidden Particles (SHiP) at the CERN SPS*, [1504.04956](#).
- [41] S. Alekhin et al., *A facility to Search for Hidden Particles at the CERN SPS: the SHiP physics case*, *Rept. Prog. Phys.* **79** (2016) 124201 [[1504.04855](#)].
- [42] SHiP collaboration, *The SHiP experiment at the proposed CERN SPS Beam Dump Facility*, *Eur. Phys. J. C* **82** (2022) 486 [[2112.01487](#)].
- [43] A. Abada, D. Bečirević, O. Sumensari, C. Weiland and R. Zukanovich Funchal, *Sterile neutrinos facing kaon physics experiments*, *Phys. Rev. D* **95** (2017) 075023 [[1612.04737](#)].
- [44] T. Li, X.-D. Ma and M.A. Schmidt, *Implication of  $K \rightarrow \pi\nu\bar{\nu}$  for generic neutrino interactions in effective field theories*, *Phys. Rev. D* **101** (2020) 055019 [[1912.10433](#)].
- [45] G. Zhou, *Light sterile neutrinos and lepton-number-violating kaon decays in effective field theory*, *JHEP* **06** (2022) 127 [[2112.00767](#)].
- [46] E. Fernández-Martínez, M. González-López, J. Hernández-García, M. Hostert and J. López-Pavón, *Effective portals to heavy neutral leptons*, *JHEP* **09** (2023) 001 [[2304.06772](#)].
- [47] A.J. Buras, *Weak Hamiltonian, CP violation and rare decays*, in *Les Houches Summer School in Theoretical Physics, Session 68: Probing the Standard Model of Particle Interactions*, pp. 281–539, 6, 1998 [[hep-ph/9806471](#)].
- [48] PARTICLE DATA GROUP collaboration, *Review of Particle Physics*, *PTEP* **2022** (2022) 083C01.
- [49] NA62 collaboration, *Search for heavy neutral lepton production in  $K^+$  decays to positrons*, *Phys. Lett. B* **807** (2020) 135599 [[2005.09575](#)].
- [50] G. Bernardi et al., *Further limits on heavy neutrino couplings*, *Phys. Lett. B* **203** (1988) 332.

- [51] T2K collaboration, *Search for heavy neutrinos with the T2K near detector ND280*, *Phys. Rev. D* **100** (2019) 052006 [1902.07598].
- [52] PIENU collaboration, *Improved search for heavy neutrinos in the decay  $\pi \rightarrow e\nu$* , *Phys. Rev. D* **97** (2018) 072012 [1712.03275].
- [53] L.D. Corpe, “Update on (pro)ANUBIS detector proposal: [https://indico.cern.ch/event/1216822/contributions/5449255/attachments/2671754/4631593/LCORPE\\_LLWorkshop2023\\_ANUBIS\\_June2023.pdf](https://indico.cern.ch/event/1216822/contributions/5449255/attachments/2671754/4631593/LCORPE_LLWorkshop2023_ANUBIS_June2023.pdf).”, June, 2023.
- [54] T.P. Satterthwaite, *Sensitivity of the ANUBIS and ATLAS Detectors to Neutral Long-Lived Particles Produced in pp Collisions at the Large Hadron Collider*, Master’s thesis, 2022.
- [55] FASER collaboration, *First Direct Observation of Collider Neutrinos with FASER at the LHC*, **2303.14185**.
- [56] FASER collaboration, *First Physics Results from the FASER Experiment*, in *57th Rencontres de Moriond on Electroweak Interactions and Unified Theories*, 5, 2023 [2305.08665].
- [57] L. Lee, C. Ohm, A. Soffer and T.-T. Yu, *Collider Searches for Long-Lived Particles Beyond the Standard Model*, *Prog. Part. Nucl. Phys.* **106** (2019) 210 [1810.12602].
- [58] T. Pierog, I. Karpenko, J.M. Katzy, E. Yatsenko and K. Werner, *EPOS LHC: Test of collective hadronization with data measured at the CERN Large Hadron Collider*, *Phys. Rev. C* **92** (2015) 034906 [1306.0121].
- [59] C. Baus, T. Pierog and R. Ulrich, “Cosmic Ray Monte Carlo (CRMC): <https://web.ikp.kit.edu/rulrich/crmc.html>.”, June, 2023.
- [60] I. Krasnov, *DUNE prospects in the search for sterile neutrinos*, *Phys. Rev. D* **100** (2019) 075023 [1902.06099].
- [61] D. Dercks, J. De Vries, H.K. Dreiner and Z.S. Wang, *R-parity Violation and Light Neutralinos at CODEX-b, FASER, and MATHUSLA*, *Phys. Rev. D* **99** (2019) 055039 [1810.03617].
- [62] D. Dercks, H.K. Dreiner, M. Hirsch and Z.S. Wang, *Long-Lived Fermions at AL3X*, *Phys. Rev. D* **99** (2019) 055020 [1811.01995].
- [63] M. Hirsch and Z.S. Wang, *Heavy neutral leptons at ANUBIS*, *Phys. Rev. D* **101** (2020) 055034 [2001.04750].
- [64] R. Beltrán, G. Cottin, M. Hirsch, A. Titov and Z.S. Wang, *Reinterpretation of searches for long-lived particles from meson decays*, *JHEP* **05** (2023) 031 [2302.03216].
- [65] H.K. Dreiner, D. Köhler, S. Nangia, M. Schürmann and Z.S. Wang, *Recasting bounds on long-lived heavy neutral leptons in terms of a light supersymmetric R-parity violating neutralino*, *JHEP* **08** (2023) 058 [2306.14700].
- [66] R. Barouki, G. Marocco and S. Sarkar, *Blast from the past II: Constraints on heavy neutral leptons from the BEBC WA66 beam dump experiment*, *SciPost Phys.* **13** (2022) 118 [2208.00416].
- [67] W. Dekens, J. de Vries, K. Fuyuto, E. Mereghetti and G. Zhou, *Sterile neutrinos and neutrinoless double beta decay in effective field theory*, *JHEP* **06** (2020) 097 [2002.07182].

- [68] FLAVOUR LATTICE AVERAGING GROUP (FLAG) collaboration, *FLAG Review 2021*, *Eur. Phys. J. C* **82** (2022) 869 [[2111.09849](#)].
- [69] A. Falkowski, M. González-Alonso, J. Kopp, Y. Soreq and Z. Tabrizi, *EFT at FASER $\nu$* , *JHEP* **10** (2021) 086 [[2105.12136](#)].
- [70] K. Bondarenko, A. Boyarsky, D. Gorbunov and O. Ruchayskiy, *Phenomenology of GeV-scale Heavy Neutral Leptons*, *JHEP* **11** (2018) 032 [[1805.08567](#)].